Spatial distributions of iron and manganese in surface waters of the Arctic's Laptev and East Siberian seas

Naoya Kanna[1*], Kazutaka Tateyama[2], Takuji Waseda[3], Anna Timofeeva[4], Maria Papadimitraki[5, 6], Laura Whitmore[7], Hajime Obata[1], Daiki Nomura[8, 9, 10], Hiroshi Ogawa[1], Youhei Yamashita[11], Igor Polyakov[7]

[1]Atmosphere and Ocean Research Institute, The University of Tokyo, 5-1-5, Kashiwanoha, Kashiwa-shi, Chiba 277-8564 Japan

[2]Kitami Institute of Technology, Kitami Hokkaido Japan

[3]Department of Ocean Technology, Policy and Environment, Graduate School of Frontier Sciences, The University of Tokyo, Kashiwa Chiba Japan

[4]Arctic and Antarctic Research Institute

[5]National Institute of Aquatic Resources-Technical University of Denmark

[6]Department of Biology, University of Southern Denmark, 5230 Odense M, Denmark

[7]International Arctic Research Center, University of Alaska Fairbanks

[8]Arctic Research Center, Hokkaido University, Kita-21 Nishi-11, Kita-ku, Sapporo-shi, Hokkaido 001-0021, Japan

[9]Global Station for Arctic Research, Global Institution for Collaborative Research and Education, Hokkaido University, Kita-21 Nishi-11, Kita-ku, Sapporo-shi, Hokkaido 001-0021, Japan

[10]Field Science Center for Northern Biosphere, Hokkaido University, 3-1-1 Minato-cho, Hakodate-shi, Hokkaido 041-0821, Japan

[11]Faculty of Environmental Earth Science, Hokkaido University, Kita-10 Nishi-5, Kita-ku, Sapporo, Hokkaido 060-0810, Japan

Correspondence to: Naoya Kanna (nkanna@g.ecc.u-tokyo.ac.jp)

Atmosphere and Ocean Research Institute, The University of Tokyo

Abstract. The Arctic Laptev and East Siberian Seas (LESS) have high biogeochemical activity. Nutrient inputs associated with river runoff and shelf sediment-water exchange processes are vital for supporting primary production in the LESS. Relative to macronutrients, data on dissolved iron (dFe) and manganese (dMn), which are essential micronutrients for primary producers, have historically been sparse for LESS. Some dFe and dMn are reportedly carried in the Central Arctic by the Transpolar Drift, a major current that directly transports Eurasian shelf water, river water, and sea ice from the LESS continental margins. However, the supply of dFe and dMn to the surface waters of the LESS and the subsequent biogeochemical processes are not well constrained. In the summer of 2021, we investigated the following questions: *what are the sources of dFe and dMn to the surface layer* and *what factors control their concentrations and distributions on the LESS continental margins*? We demonstrated strong regional controls on dFe and dMn distributions based on distinct hydrographic regimes between the eastern side of the LESS (East Siberian Sea and Chukchi Abyssal Plain) and the western side (Makarov and Amundsen basins). Specifically, the East Siberian Sea and Chukchi Abyssal Plain were governed by Pacific-sourced water, and the Makarov and Amundsen basins were influenced by Atlantic-sourced water. Pacific-sourced water contained higher levels of dMn released from continental shelf sediments than Atlantic-sourced water. In contrast, elevated dFe signals were not observed, likely because sedimentary dFe was more rapidly removed from the water column through oxidation or scavenging than dMn. The impact of river water discharge on the dFe distributions of Pacific- and Atlantic-sourced water was significant. A positive correlation between the fraction of meteoric water (river water and precipitation), dFe, and humic-like colored dissolved organic matter (CDOM) in these waters confirmed that dFe and CDOM are common freshwater sources. Terrigenous organic ligands likely stabilize Fe in the dissolved phase, which is not the case for Mn. Sea-ice melting and formation were not significant sources during the observation period. We conclude that the major sources controlling the dFe and dMn distributions in the LESS continental margins are river discharge and shelf sediment input.

1 Introduction

The Arctic Laptev and East Siberian Seas (LESS) are strongly influenced by ongoing changes in the Arctic climate. The LESS has shown a drastic increase in net primary production in recent decades, as evidenced by satellite records (Lewis et al., 2020) as the region has warmed (Rantanen et al., 2022) and seasonal ice coverage has decreased (Fox-Kemper et al., 2021; Sumata et al., 2023). Since the middle of the 2010s, the increased penetration of Atlantic Water into the LESS continental margins has driven "Atlantification," which weakened oceanic stratification, enhanced upward fluxes of heat and nutrients due to the increased vertical mixing, and reduced sea ice coverage (Polyakov et al. 2017, 2020, 2023). Given the increasing trend in the discharge of Eurasian rivers (Feng et al., 2021), the export of terrestrial materials, including nutrients and trace metals, to LESS might intensify, potentially affecting biological production and carbon deposition on the shelves. The fluxes of shelf-derived materials from LESS to the Central Arctic have likely increased over the past decade (Kipp et al., 2018). Moreover, Arctic sea ice often contains sediments entrained in the East Siberian Arctic Shelf (Eiken et al., 2000, 2005; Hölemann et al., 1999a;

Krumpen et al., 2020; Waga et al., 2022; Wegner et al., 2017), such that the decreasing trend in seasonal ice coverage might affect material fluxes to the Central Arctic upon melting. Therefore, LESS is a key region for understanding how climate change impacts biogeochemical cycling in the Arctic Ocean.

Iron (Fe) and manganese (Mn) are essential micronutrients for primary producers and are involved in important phytoplankton metabolic pathways (Morel and Price, 2003; Twining and Baines, 2013). Fe and Mn are supplied to surface waters from common sources, such as the porewaters of shelf sediments (Cid et al., 2012; Jensen et al., 2020; Kondo et al., 2016), sea ice meltwater (Bolt et al., 2020; Evans and Nishioka, 2019; Hölemann et al., 1999a, 1999b), and river water (Guieu et al., 1996; Pokrovsky et al., 2016; Savenko and Pokrovsky, 2019). When paired, the Fe and Mn concentrations can often be used as indicators of common-source fluxes (Jensen et al., 2020; Landing and Bruland, 1987). Ongoing changes in LESS may intensify the supply of Fe and Mn to surface waters in the Central Arctic. Some Fe and Mn derived from these sources are transported to the Central Arctic by the Transpolar Drift, a major current that directly transports Eurasian shelf water, river water, and sea ice from the LESS (Charette et al., 2020; Gerringa et al., 2021). A few studies have indicated the importance of Lena River runoff and sea ice melt on Fe and Mn distributions near the Laptev Sea (Hölemann et al., 1999, 2005; Klunder et al., 2012; Middag et al., 2011). However, LESS is still one of the least studied areas of the Arctic Ocean in terms of trace metal dynamics. In particular, limited data on trace metals have been reported over the East Siberian Sea.

This study reports the spatial distributions of Fe and Mn in the surface waters of the LESS, including the East Siberian Sea, Chukchi Abyssal Plain, Makarov Basin, and Amundsen Basin. Observations were made in international cooperation with the Nansen and Amundsen Basin Observational System (NABOS) expedition during the late summer of 2021 in the Arctic Ocean. A detailed water mass analysis was performed to clarify the potential sources of Fe and Mn in surface LESS. Sea ice cores were also collected to calculate Fe and Mn sea ice inventories, and the potential supply to the surface ocean upon melting was evaluated. Moreover, we investigated the interaction of dissolved organic matter with Fe and Mn in the LESS. By combining these datasets, we interpreted the factors controlling the concentrations and distributions of Fe and Mn on the surface of LESS.

2 Materials and Methods

2.1 Shipboard sampling

Observations in the LESS were conducted onboard the Russian Research Vessel *Akademik Tryoshnikov* from September to October 2021 (Fig. 1a). Low-density polyethylene (LDPE) bottles and buckets (Thermo Fisher Scientific, USA), polyethylene bags (GL Sciences, Japan), AcroPak capsules with Supor membrane filters (0.8/0.2 μm pore size, Pall, USA), and a Tygon tube (Masterflex, Germany) used for sampling trace metals were thoroughly acid-cleaned in a class-100 clean-air laboratory. Seawater was collected from a depth of approximately 10 m from the side of the ship using a peristaltic pump (Geopump, Geotech Environmental Equipment, USA) and a Tygon tube. Filtered and unfiltered Fe and Mn samples were obtained to assess their labile particulate fractions. Samples of the dissolved fractions of Fe and Mn (dFe and dMn) were collected in

LDPE bottles after filtration through AcroPak filters connected to Tygon tubes. Samples for total acid dissolvable Fe and Mn (TdFe and TdMn) were collected into LDPE bottles without filtration. The pH of the Fe and Mn samples was adjusted to < 1.8 by adding ultrapure-grade 6 M hydrochloric acid (Tamapure AA-100, Tama Chemicals, Japan), and were stored for a year before the analysis. Therefore, the concentration differences between the unfiltered (i.e., TdFe and TdMn) and filtered (i.e., dFe and dMn) samples were attributed to the acid-labile particulate fraction. Samples for nutrient analysis were collected in acrylic vials after filtration. Samples for dissolved organic matter (DOM) were collected into pre-combusted (450°C for 5 h) glass bottles after filtration through pre-combusted glass fiber filters (0.7 μm nominal pore size, Whatman GF/F, UK). The samples for stable isotope of oxygen ($\delta^{18}O$) in the seawater were collected into glass bottles with rubber inserts in the caps. The samples for nutrients and DOM were frozen immediately after collection at −20ºC and were shipped back to the onshore laboratory.

The water properties at depths of 0–30 m were measured using a portable CTD sensor (RINKO 102, JFE Advantech, Japan) and are shown in a temperature versus salinity diagram (Fig. S1). Full-depth temperature and salinity profiles were obtained using a Seabird SBE911plus CTD system (Figs. S2 and S3).

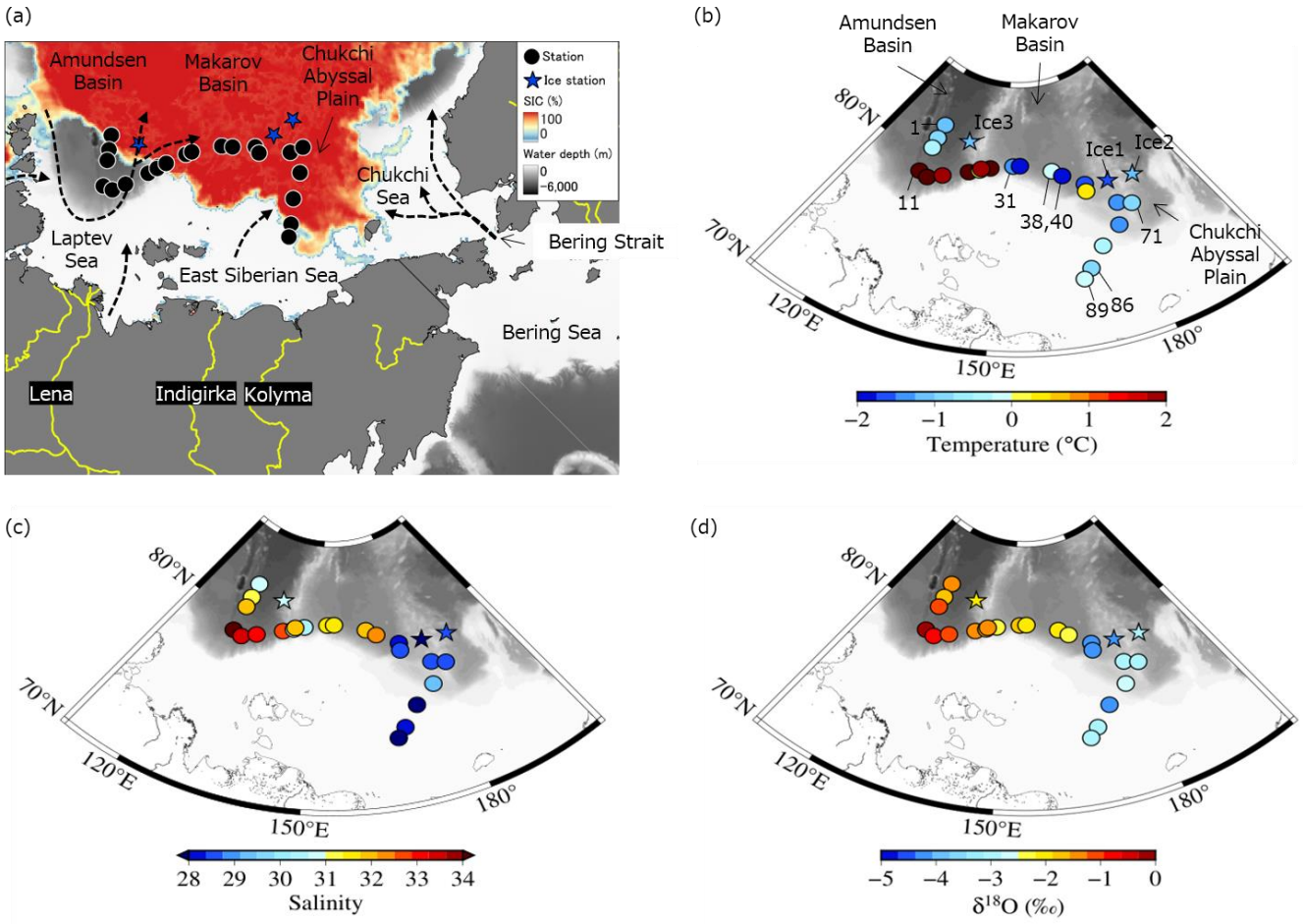

105 **Figure 1** (a) Location of stations sampled in the Arctic's Laptev and East Siberian Seas (LESS) in the late summer of 2021. Spatial distributions of (b) water temperature, (c) salinity, and (d) $\delta^{18}O$ in the surface. Sea ice concentration (SIC, %) on 1 October 2021 (GCOM-W/AMSR2, Japan Aerospace Exploration Agency) and general water flow on the surface of LESS (Anderson et al., 2015; Bauch et al., 2018; Clement Kinney et al., 2022; Doglioni et al., 2022; Rudels et al., 2004; Stabeno et al., 2018) are depicted in (a).

110 **2.2 Sampling on sea ice and sample processing**

Sea ice observations were conducted at three ice stations on October 1st (St. Ice 1), 2nd (St. Ice 2), and 10th (St. Ice 3), 2021 (Fig. 1a-b). Water sampling under sea ice was performed to analyze Fe, Mn, nutrients, DOM, and $\delta^{18}O$ at depths of 1, 5, and 10 m using the pump system described in Sect. 2.1. Sea ice cores were collected using an ice corer (Mark II Coring System, Kovacs Enterprise, USA) and sectioned into five subsamples using a titanium flat-headed screwdriver. The subsamples were

115 cleaned on-site by removing more than 2 cm of their outer layers using acid-cleaned ceramic knives, according to previously

reported methods (Evans and Nishioka, 2019; Kanna et al, 2014). The cleaned ice samples were transferred to LDPE buckets. Snow samples were collected in polyethylene bags by using an acid-cleaned polycarbonate scoop. The snow and cleaned ice samples were melted inside a class-100 clean-air bench onboard the laboratory. The meltwaters for Fe, Mn, nutrients, DOM, and $\delta^{18}O$ analyses were subsampled and processed as described in Sect. 2.1. The salinity of the meltwater samples was measured using a portable salinity sensor (Multi 3510; Xylem, USA).

2.3 Sample analysis

The acidified water samples for Fe and Mn analyses were preconcentrated using a manual solid-phase extraction system equipped with a Nobias Chelate-PA1 resin column (Hitachi High Technologies, Japan) (Sohrin et al., 2008; Kondo et al., 2016; Kanna et al., 2022). Ultrapure-grade nitric acid, acetic acid, and ammonium solution (Tamapure AA-100, Tama Chemicals, Japan) were used for pre-concentration and extraction. The water samples were adjusted to pH 6.0 ± 0.1 by adding a 3.6 M ammonium acetate buffer solution prepared from acetic acid and ammonium solution. Fe and Mn concentrated on the resin were eluted with 2 M nitric acid and analyzed using high-resolution inductively coupled plasma mass spectrometry (ELEMENT XR, Thermo Fisher Scientific, USA). Procedure blanks of Fe and Mn were evaluated using ultrapure water following the pre-concentration procedures, that showed 0.13 ± 0.04 nmol kg^{-1} (n = 84) for Fe and 0.002 ± 0.005 nmol kg^{-1} (n = 84) for Mn, respectively. Certified reference materials for trace metals, NASS-7 and CASS-6 (National Research Council of Canada) were used to validate the pre-concentration procedures. The analytical values were within the error range of the certified reference materials (Table 1).

Dissolved organic carbon (DOC) was analyzed using a total organic carbon analyzer (TOC-L, Shimadzu, Japan). Absorbance spectra for chromophoric dissolved organic matter (CDOM) were analyzed between 200 and 800 nm at 1 nm intervals using a dual-beam spectrophotometer (UV-1800, Shimadzu, Japan) with a 1 cm quartz-windowed cell. The sample spectra were corrected using ultrapure water spectra and converted to Napierian absorption coefficients at wavelength (a (λ), m^{-1})(Green and Blough, 1994).

The excitation–emission matrix fluorescence spectra of the CDOM were analyzed using a fluorescence spectrophotometer (FP-8500, JASCO, Japan). Spectra were obtained at excitation wavelengths ranging from 250 to 500 nm and emission wavelengths ranging from 280 to 600 nm. The fluorescence intensity was corrected to the area under the Raman peak of ultrapure water (excitation wavelength = 350 nm) and calibrated to Raman units (RU) using the methods outlined by Lawaetz and Stedmon (2009) and Tanaka et al. (2016).

The $\delta^{18}O$ value of the water samples was determined using an isotope water analyzer (Picarro L2120-i, Picarro, USA) with an analytical precision of ±0.3‰. Macronutrient concentrations were determined using an autoanalyzer (QuAAtro, BL TEC, Japan) with a continuous-flow system. The measurements were calibrated using seawater as a reference (KANSO Technos, Japan).

2.4 CDOM characterization

The CDOM absorption coefficient at 350 nm (a_{350}) was used to indicate terrestrial humic substances. In addition, parallel factor analysis (PARAFAC) was applied to statistically decompose the excitation–emission matrix fluorescence spectra into their components. PARAFAC was performed in MATLAB (MathWorks, Natick, MA, USA) using the DOMFluor toolbox (Stedmon and Bro, 2008). The dataset used in this study comprises 42 samples of seawater, snow, and sea ice. A brine sample (n = 1) was assessed as an outlier in the PARAFAC model and was not used in this study. The wavelengths for PARAFAC were obtained at excitation wavelengths ranging from 250 to 500 nm and emission wavelengths ranging from 280 to 535 nm. The correct number of components was primarily determined using split-half analysis and random initialization (Stedmon and Bro, 2008). The three-component model was validated by using the PARAFAC model (Fig. S4). Components 1 and 2 exhibit fluorescence peaks in the visible region, defined as visible fluorescence. Component 1 peaks at an emission wavelength of 410 nm and is traditionally categorized as a humic-like fluorophore of marine origin (Coble, 1996). Component 2 peaks at an emission wavelength of 470 nm and is traditionally categorized as a humic-like fluorophore of terrestrial origin (Coble, 1996), although it has been reported that marine microbes produce this type of fluorophore (Goto et al., 2020). In this study, component 1 was combined with component 2 and interpreted as all humic-like fluorophores because their fluorescence intensities were not very different among the sampling locations. Component 3 exhibits fluorescence peaks in the ultraviolet A (UVA) region, defined as UVA fluorescence. This fluorophore is traditionally categorized as a protein-like fluorophore (Coble, 1996).

2.5 Calculation for water mass fractions

To quantify the relative contribution of freshwater to changes in the surface water properties of LESS, we assumed a mixture of four components: meteoric water, sea-ice meltwater, Pacific Water, and Atlantic Water. Fractions of mass, salinity, $\delta^{18}O$, and the nitrate to phosphate ratio balance equations are described using the water properties of these four endmembers (Bauch et al., 2011; Charette et al., 2020; Gerringa et al., 2021; Newton et al., 2013):

$$f_{mw} + f_{sim} + f_{Pacific} + f_{Atlantic} = 1, \quad (1)$$

$$f_{mw} \cdot S_{mw} + f_{sim} \cdot S_{sim} + f_{Pacific} \cdot S_{Pacific} + f_{Atlantic} \cdot S_{Atlantic} = S, \quad (2)$$

$$f_{mw} \cdot \delta_{mw} + f_{sim} \cdot \delta_{sim} + f_{Pacific} \cdot \delta_{Pacific} + f_{Atlantic} \cdot \delta_{Atlantic} = \delta, \quad (3)$$

$$f_{mw} \cdot P_{mw} + f_{sim} \cdot P_{sim} + f_{Pacific} \cdot P_{Pacific} + f_{Atlantic} \cdot P_{Atlantic} = P, \quad (4)$$

where f, S, δ, and P are the fractions of mass, salinity, $\delta^{18}O$, and phosphate concentration based on the nitrate-to-phosphate ratio, and the suffixes mw, sim, Pacific, and Atlantic indicate meteoric water, sea-ice meltwater, Pacific Water, and Atlantic Water, respectively (Table 2). f_{mw} includes river runoff and local precipitation. The measured values of nitrate+nitrite (N) in each sample were used to compute the individual phosphate endmembers for the Pacific and Atlantic fractions from the

Atlantic Water Line ($P = 0.0596 \times N + 0.1139$; Bauch et al., 2011) and Pacific Water Line ($P = 0.0653 \times N + 0.94$; Jones et al., 2008) for each sample. Notably, this calculation produced a slightly negative f_{Pacific} owing to inaccuracies in the endmembers and measurements (Bauch et al., 2011). Indeed, our calculation showed negative f_{Pacific} at four stations with an average of −2%. However, this error remains relatively small within the Atlantic regime and is still within the uncertainty (~10% for marine waters) of the method (Yamamoto-Kawai et al., 2008).

3 Results

3.1 Hydrography of LESS surface waters

Water properties in the East Siberian Sea and Chukchi Abyssal Plain differed significantly from those of the Makarov and Amundsen Basins in the late summer of 2021. The surface waters in the East Siberian Sea and Chukchi Abyssal Plain were relatively cold (temperature < 0°C) and fresh (salinity < 30) compared with those in the Makarov and Amundsen Basins (Figs. 1b, c, and S2). The waters in the East Siberian Sea and Chukchi Abyssal Plain were characterized by low $\delta^{18}O$ values of less than −2.5‰ (Fig. 1d). The differences among regions were likely due to the magnitude of the mixing of Pacific-sourced water with Atlantic-sourced water, river runoff, and the melting of sea ice. Pacific-sourced water enters the Bering Strait, passes through the Chukchi Sea, and penetrates the East Siberian Sea (Fig. 1a). Atlantic-sourced water enters the Amundsen Basin and flows along a continental slope (Fig. 1a). The mixed layers in the Atlantic and Pacific sectors have different geochemical and physical characteristics. In the temperature versus salinity diagram, the properties of the upper water layer (< 30 m) of the East Siberian Sea and the Chukchi Abyssal Plain (Sts. 71, 89, and Ice 1; Fig. 1b) were similar to those of the Surface Polar Mixed Water that originated in the Pacific sector of the Arctic Ocean, which is characterized by temperatures < 0 and salinity < 31 (Figs. 2 and S1). In contrast, the upper water layer found in the Makarov and Amundsen basins (Sts. 1, 11, 31, and Ice 3; Fig. 1b) is not derived from Surface Polar Mixed Water but is a product of a mixture of warm, saline Atlantic Water (temperature > 0 and salinity > 34.8) and freshwater (Figs. 2 and S1).

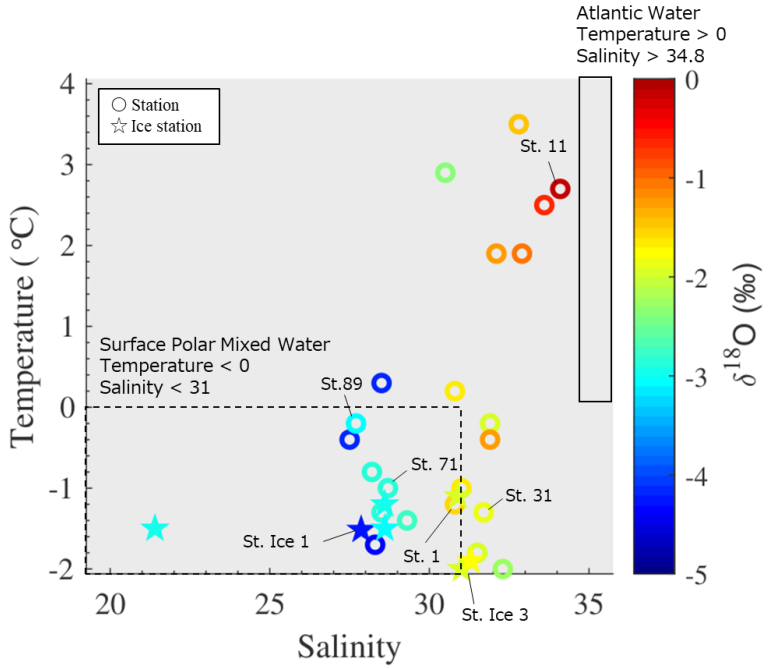

Figure 2 Temperature versus salinity diagram on the surface with stations sampled in the Arctic's Laptev and East Siberian seas. The color scale shows the $\delta^{18}O$ values in each water sample. The temperature and salinity ranges of Surface Polar Mixed and Atlantic waters are indicated by the area surrounded by dashed and solid lines, respectively.

The surface water in the East Siberian Sea and Chukchi Abyssal Plain was generally enriched in silicate and Mn, but depleted in Fe relative to the Makarov and Amundsen basins (Fig. 3a−e). The concentrations of silicate and TdMn reached 8.9 μmol L^{-1} and 83.5 nmol kg^{-1}, respectively and the concentration of TdFe was as low as 0.9 nmol kg^{-1} in the East Siberian Sea and Chukchi Abyssal Plain. The TdFe concentration tended to be high along the continental slope (Fig. 3d and e), with a maximum value of 79.2 nmol kg^{-1}. Differences between the Fe and Mn distributions were also observed at two shallow (~ 40 m bottom depth) southernmost stations on the shelf of the East Siberian Sea (Sts. 86 and 89; Fig. 3). The TdFe concentrations were relatively low (1.58−1.62 nmol kg^{-1}) at the stations where the notably high TdMn were detected (70.7−83.5 nmol kg^{-1}). dFe and dMn, which did not include particles, exhibited spatial variations similar to those of TdFe and TdMn. The concentration differences between the unfiltered (i.e., TdFe and TdMn) and filtered (i.e., dFe and dMn) samples are attributed to the acid-labile particulate fractions of these metals. The acid-labile particulate fractions of Fe accounted for 48%–61% of TdFe but only 6%–18% of TdMn at the stations on the shelf. These results indicate that Fe was relatively hosted in the particulate phase and Mn in the dissolved phase on the shelf. Various DOC concentrations were observed at different sampling locations (Fig. 3f) and exceeded 100 μmol L^{-1} at most stations. The detailed DOC distributions are discussed along with the optical information of the CDOM in Sect. 4.3.

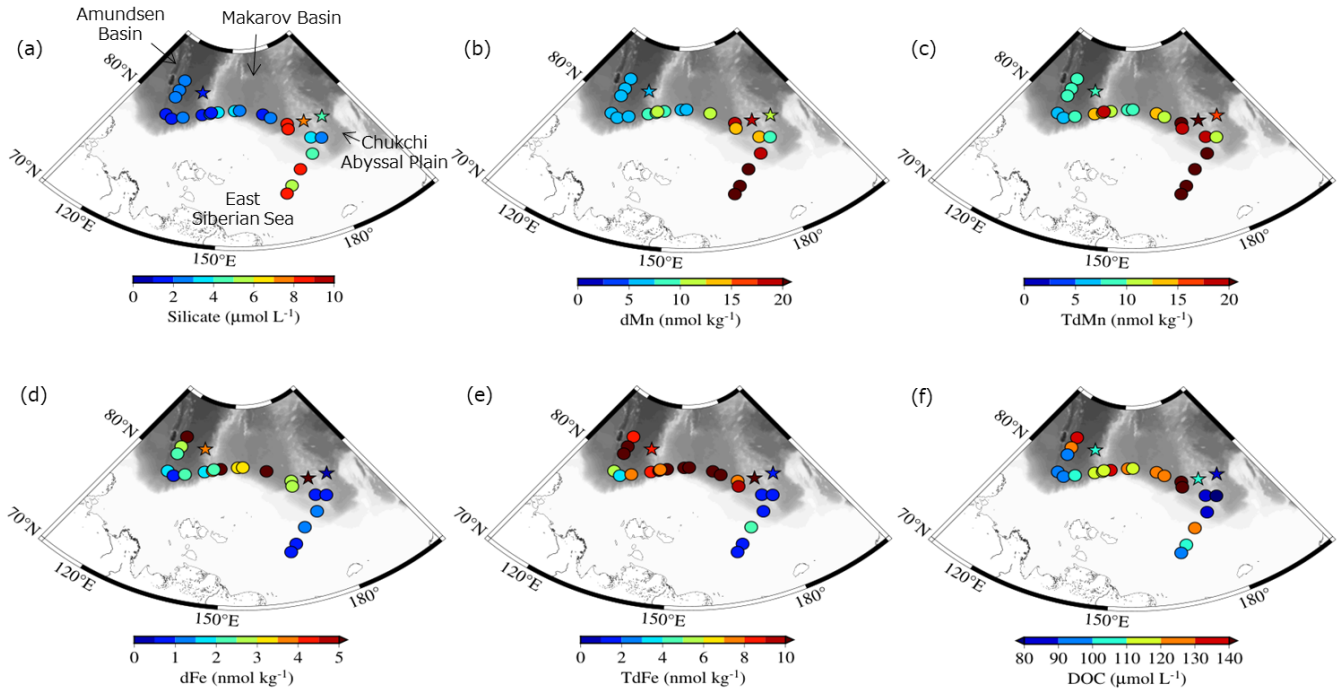

Figure 3 Spatial distributions of (a) silicate, (b) dMn, (c) TdMn, (d) dFe, (e) TdFe, and (f) DOC in the surface of the Arctic's Laptev and East Siberian seas.

3.2 Water mass analysis

The mass fractions of the Pacific Water ($f_{Pacific}$), Atlantic Water ($f_{Atrantic}$), sea ice meltwater (f_{sim}), and meteoric water (f_{mw}) components computed by solving Equations (1)–(4) are shown in Fig. 4g–i. The $f_{Pacific}$ was greater than 50% in the surface waters of the East Siberian Sea and Chukchi Abyssal Plain and less than 20% in the Makarov Basin (Fig. 4a). Small values of $f_{Pacific}$ (up to 2%) were observed in the Amundsen Basin. At this location, however, the $f_{Pacific}$ signal does not originate from Pacific-sourced water but from water modifications by denitrification within the sediment over the Laptev Shelf (Bauch et al., 2011). A negative or positive value of f_{sim} indicates the addition of brine or meltwater to the surface layer (Fig. 4c). The f_{sim} value in the surface water was as high as 5.8% over the East Siberian Sea and 3.4% over the Amundsen Basin (Fig. 4c), where the melting of sea ice was likely predominant. In contrast, a negative value of f_{sim} in the Makarov Basin suggests that sea ice formation is dominant, which agrees with previous studies (Bauch et al., 2011; Yamamoto-Kawai et al., 2005). The f_{mw} in the surface water increased by approximately 20% from west to east (Fig. 4d). The long-term trend of f_{mw} has increased in the Pacific sector of the Arctic Ocean since 1981 (Polyakov et al., 2020), which may be attributed to the influence of Siberian river runoff or increased freshwater flux through the Bering Strait.

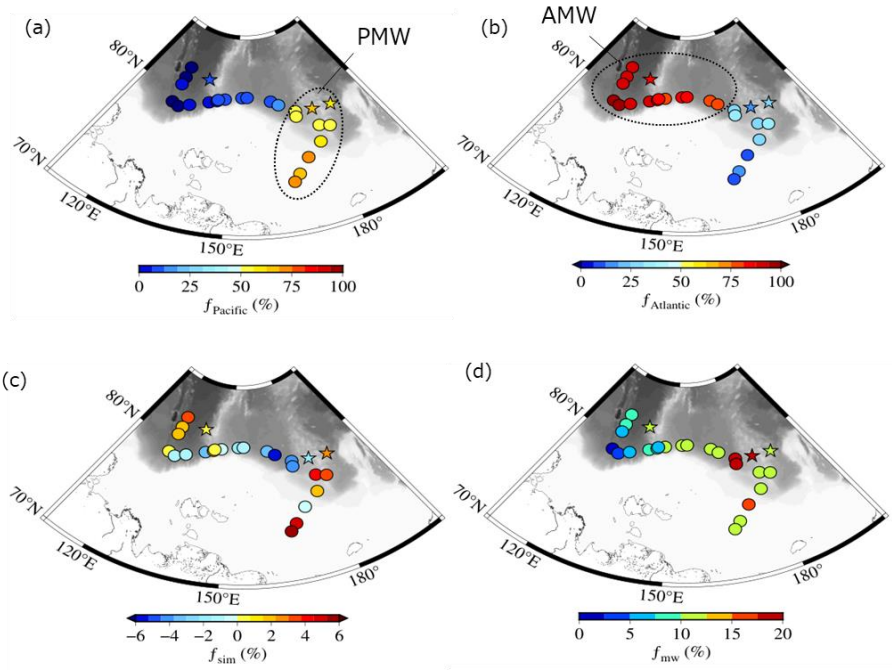

235

Figure 4 Spatial distributions of fractional (a) Pacific Water ($f_{Pacific}$), (b) Atlantic Water ($f_{Atlantic}$), (c) sea ice meltwater (f_{sim}), and (d) meteoric water (f_{mw}) in the surface of the Arctic's Laptev and East Siberian Seas. Abbreviations in (a) and (b): Surface Polar Mixed Water (PMW) and Surface Atlantic Mixed Water (AMW).

3.3 Physical and chemical properties of sea ice

240 During the NABOS expedition in the late summer of 2021, snow, sea ice, and under-ice water were collected from three ice stations (Fig. 1). Detailed observations of the ice cores and snow pits at these stations can be found in the NABOS 2021 Cruise Report (https://uaf-iarc.org/nabos-products/). Thin-section analysis of a single ice core collected at St. Ice 2 revealed that the sea ice was composed of approximately 9% granular ice, 37% columnar ice, and 54% mixed ice (Fig. S5). Salinity and $\delta^{18}O$ values in the sea ice were similar among stations, ranging from 0 to 3.8 and from −3.6 to 0‰, respectively (Fig. 5a-b).
245 Generally, Fe and Mn concentrations in the sea ice were lower than those in the under-ice water, except for the ice section (0.2 m from the bottom) collected at St. Ice 3 (Fig. 5c−f). The dFe concentrations in the sea ice gradually decreased from 3.2 to 1.7 nmol kg^{-1} with the ice core depth, while the dMn concentrations increased from 2.4 to 5.2 nmol kg^{-1}. The TdFe and TdMn concentrations exhibited vertical variations, similar to those of the dissolved fractions. The TdFe concentration tended to be higher in snow samples than in sea ice and under-ice water; however, this did not apply to TdMn.
250 We calculated the inventories of Fe and Mn from the cumulative metal loads of the 110 cm ice cores collected at St. Ice 1 (Table 3). The metal inventory of the ice core was comparable to that obtained from the Canada Basin (Evans and Nishioka, 2019) except for TdFe, which had a lower inventory. Moreover, the reported particulate Fe inventory in the ice core from the

Western-Central Arctic Ocean (Bolt et al., 2020) exceeded the TdFe inventory in this study. Such discrepancies are likely due to greater heterogeneity in the distribution of particulate Fe loads in Arctic pack ice (Bolt et al., 2020). The sediment loadings of the collected ice samples were low based on visual observations, such that there was no evidence of ice-rafted sediment adding Fe and Mn to the surface waters, although their importance has been reported (Hölemann et al., 1999a, 1999b; Measures, 1999; Rogalla et al., 2022; Tovar-Sánchez et al., 2010).

The DOC concentration varied in the snow (24.5−105 μmol L^{-1}) and sea ice samples (32.1−147 μmol L^{-1}), while the concentrations were relatively uniform vertically in the under-ice water (84−110 μmol L^{-1}) (Fig. 5g). The optical properties of the CDOM showed that the intensities of visible fluorescence were lower in snow and sea ice than in the under-ice water (Fig. 5h). The intensity of UVA fluorescence was relatively high in sea ice at St. Ice 2 but not at St. Ice 1 (Fig. 5i). Macronutrients were generally depleted in the sea ice, except for nitrate+nitrite at St. Ice 2, which showed enrichment of 1.3 μmol L^{-1} compared to the under-ice water (< 0.25 μmol L^{-1}) (Fig. 5j–l). The enrichment of nitrate+nitrite was also observed in the snow samples (1.2 μmol L^{-1}).

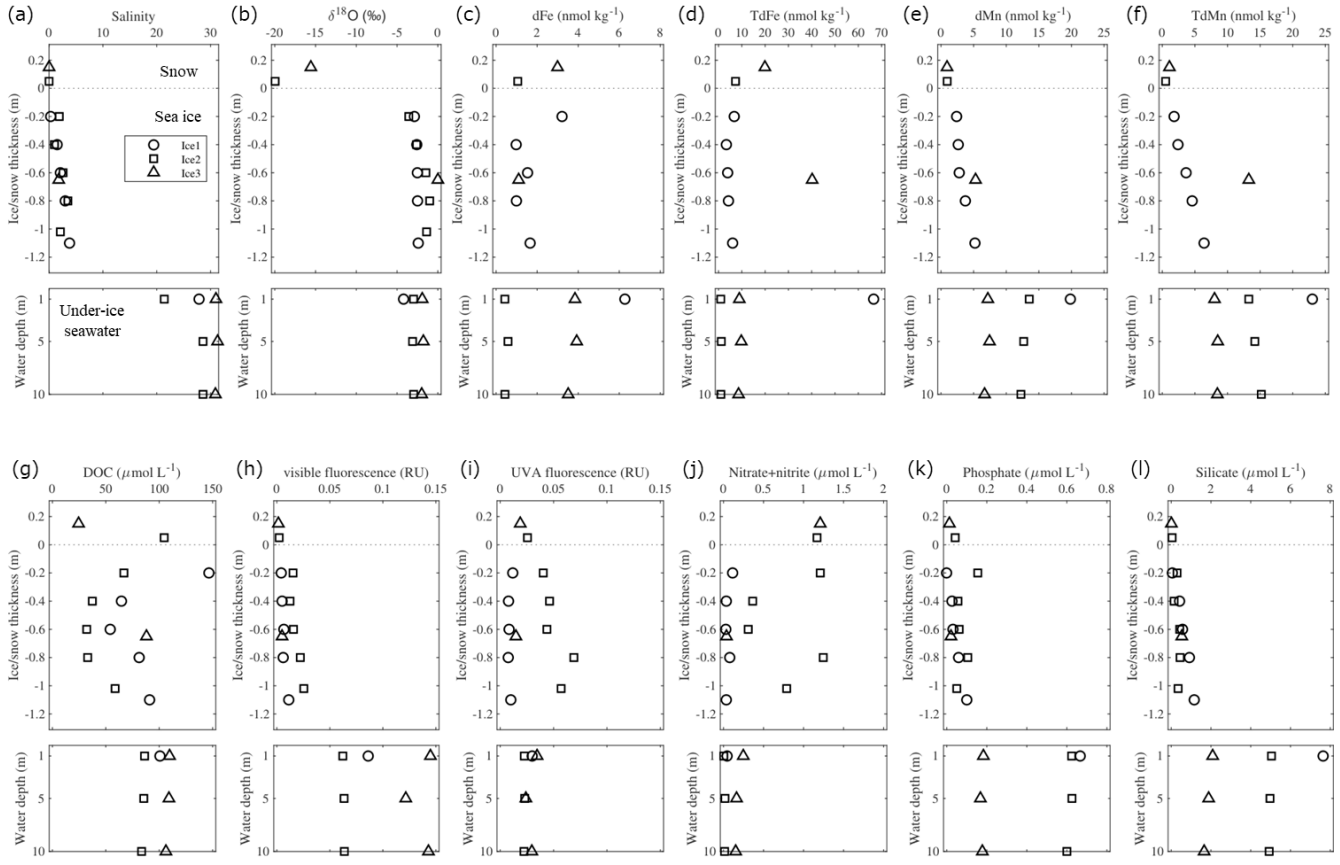

Figure 5 Vertical profiles of (a) salinity, (b) $\delta^{18}O$, (c) dFe, (d) TdFe, (e) dMn, (f) TdMn, (g) DOC, (h) visible fluorescence, (i) UVA fluorescence, (j) nitrate+nitrite, (k) phosphate, and (l) silicate in snow, sea ice, and under-ice water, respectively.

4 Discussion

4.1 Comparison of Fe and Mn concentrations in seawater and freshwater sources

Variations of salinity and $\delta^{18}O$ value in the surface water of LESS continental margins are attributed to local precipitation or river runoff and melting/formation of sea ice. Figure 6 shows the salinity versus $\delta^{18}O$ diagram based on the samples of surface water, snow, sea-ice meltwater, and the previously reported freshwater sources (Evans and Nishioka, 2019; Marsay et al., 2019; Peterson et al., 2016). The salinity and $\delta^{18}O$ values in most surface water samples deviated from the meteoric endmember, including snow meltwater and the Siberian rivers. However, the salinity and $\delta^{18}O$ values in the under-ice water at St. Ice 2 rather deviated toward the sea-ice endmember, resulting from substantial input of sea-ice meltwater into the station.

The dMn concentration in the surface water gradually increased with decreasing salinity (Fig. 6b). The dFe concentration also showed a similar increasing trend in salinity ranges from 31 to 34 (Fig. 6a); however, the dFe concentration in less saline waters (salinity < 31) was independent of salinity variation. Previous studies have shown that notably high dFe and dMn concentrations in the Siberian rivers as having 1751 ± 1218 nmol L^{-1} and 208 ± 279 nmol L^{-1}, respectively (Peterson et al., 2016), such that river waters must have supplied substantial amounts of Fe and Mn into the surface of LESS. In contrast, dFe and dMn concentrations in the sea-ice endmember were relatively low (2.0 ± 1.3 nmol kg^{-1} for dFe; 5.3 ± 3.3 nmol kg^{-1} for dMn). The enriched dMn in the under-ice water at St. Ice 2 (13.5 nmol kg^{-1}) was not likely derived from the input of sea ice meltwater because of the low level of dMn in the sea-ice endmember, suggesting the existence of extra Mn sources in the surface water. In the subsequent section, we discuss the factors controlling the distribution of Fe and Mn on the surface of LESS.

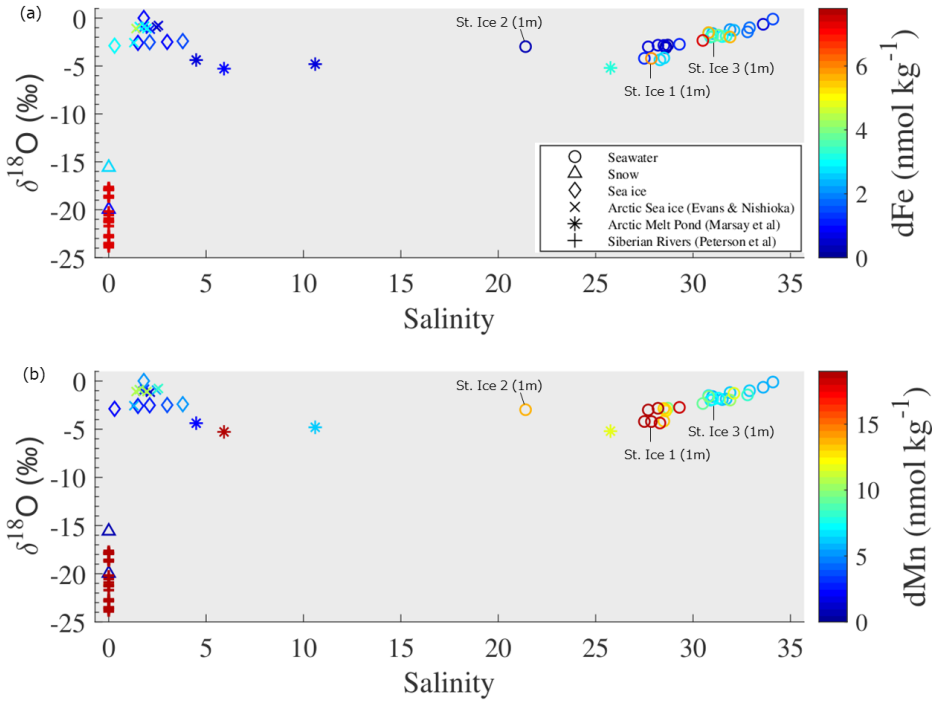

Figure 6 Salinity versus $\delta^{18}O$ diagram in seawater, snow, and sea ice. The color scale shows concentrations of (a) dFe and (b) dMn in each water sample. The values of other freshwater sources are cited by Evans and Nishioka (2019), Marsay et al. (2018), and Peterson et al. (2016).

4.2 Potential sources of Fe and Mn in the surface LESS

Based on the water mass analysis described in Sect. 3.2, we classified the surface water into Surface Polar Mixed Water (PMW) and Surface Atlantic Mixed Water (AMW) (Fig. 4a-b, dotted circle borders the area). The PMW contains a large fraction of Pacific-sourced water ($f_{Pacific}$ > 50%) and is mostly found in the East Siberian Sea and Chukchi Abyssal Plain, whereas the AMW is found in the Makarov and Amundsen Basins. The PMW is generally characterized by high silicate, low Fe, and high Mn concentrations relative to AMW (Fig. 3a−e). The high silicate content of the PMW likely resulted from nutrient-rich Pacific Water entering the shallow Bering Strait (Chen et al., 2018; Jensen et al., 2020; Nishino et al., 2013). The maximum surface silicate concentration along the continental margin of the western Makarov Basin, which is a typical signature of runoff from the Lena River in the region (Alling et al., 2010; Anderson et al., 2017), was not observed in this study (Fig. 3a).

A significant correlation between dFe and dMn has been observed in the deeper waters (>3000 m) of the Amundsen and Makarov basins because scavenging removal is the dominant process in deep-water masses (Klunder et al., 2012). In the LESS surface water, Fe was not correlated with Mn in the unfiltered and filtered fractions (Fig. S6). Additional factors, such as external inputs, influence the distribution of dFe and dMn in surface waters, leading to the disappearance of the Fe-Mn

relationship. Moreover, the enrichment of dMn compared to that of dFe (Fig. S6a) was observed in all sampled surface waters, suggesting the importance of the input fluxes of dMn or the preferential scavenging of dFe relative to dMn. Fe and Mn are redox-active metals that share common sources in surface water, such as sediments, dust deposition, and freshwater inputs. The dust deposition is considered to be of minor importance in the LESS, given the relatively low concentrations of TdFe (~19.9 nmol kg^{-1}) and TdMn (~1.1 nmol kg^{-1}) observed in the snow samples in this study (Fig. 5d and f). In general, the summertime atmospheric deposition fluxes of Fe and Mn into the Arctic Ocean are reportedly low (Kadko et al, 2016; Marsay et al, 2018), especially in comparison to Arctic rivers and coastal erosion/diagenetic fluxes from shelf sediments (Charette et al., 2020; Jensen et al., 2021; Kadko et al., 2018). In the following discussion, we evaluate the potential sources (sedimentary input, river runoff, and sea ice formation and melt) of these metals in PMW and AMW.

4.2.1 Sedimentary input

To distinguish shelf-derived Fe and Mn, parameter N^* ($N^* = 0.87\times(N-16\times P+2.9)$; Gruber and Sarmiento, 1997) was evaluated for PMW and AMW. A negative or positive value of N^* in the water indicates a nitrate deficit (denitrification) or excess nitrate (nitrogen fixation), respectively, relative to phosphate. In the Chukchi Sea, significant denitrification occurs within shelf sediments because nitrate is consumed instead of oxygen for organic matter decomposition (Yamamoto-Kawai et al., 2006). Nitrogen fixation also occurs throughout the Chukchi Sea; however, it is a minor process in the overall nitrogen cycle (Shiozaki et al., 2018). Negative N^* could indicate water passing through the reductive Chukchi Shelf and penetrating the Makarov Basin (Nishino et al., 2013). Our results showed that the N^* value in PMW was much lower (< -5) than that in AMW (Fig. 7). Although Fe and Mn are considered to be released in the dissolved phase from reductive sediments over the Chukchi Shelf, these metals are gradually removed from the water column as the particulate phase (Jensen et al., 2020). The TdMn and dMn concentrations tended to be high in the low-N^* PMW, suggesting a reductive sedimentary flux that released Mn from the Chukchi Shelf (Fig. 7b and d). Mn was more elevated at shallow shelf stations 86 and 89, which were the stations most influenced by shelf inputs. Given that the dMn to TdMn ratio in PMW is as high as 85.2 ± 10.2%, Mn was primarily in the dissolved phase. In contrast, the TdFe and dFe concentrations in the PMW were relatively low (Fig. 7a and c) compared to those typically observed in the continental margin of the Arctic Ocean (Aguilar-Islas et al., 2013; Cid et al., 2011, 2012; Jensen et al., 2020; Klunder et al., 2012; Kondo et al., 2016; Nakayama et al., 2011; Nishimura et al., 2012). This is likely because Fe is removed much more rapidly from the Chukchi Shelf water column than Mn via oxidation and re-precipitation (Jansen et al., 2020; Millero et al., 1987; Vieira et al., 2019). Indeed, we observed a lower dFe to TdFe ratio (43.6 ± 23.8%) in PMW, such that Fe was primarily in the particulate phase. The relatively high Fe concentrations at stations Ice-1, 38, and 40 are likely attributable to riverine flux because these stations show a relatively high fractional f_{mw} (see discussion below).

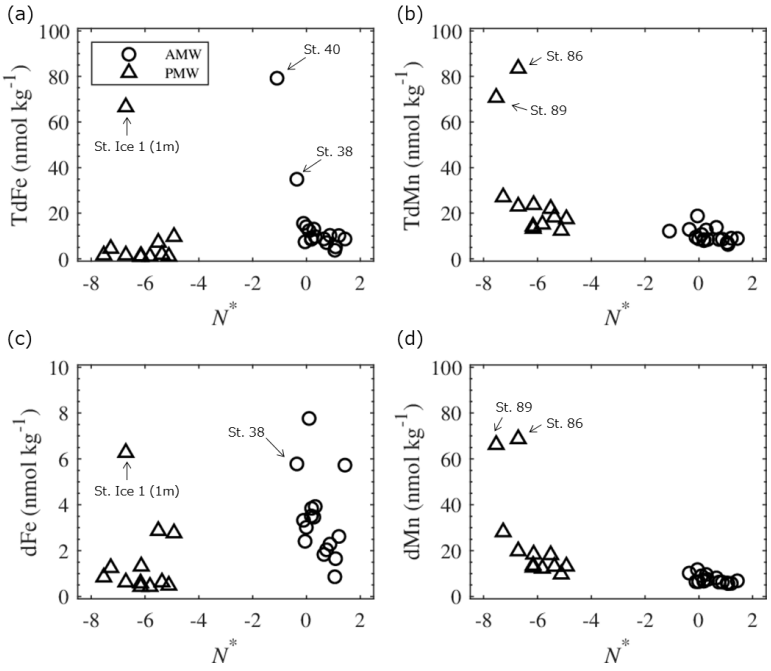

Figure 7 Plots of (a) TdFe, (b) TdMn, (c) dFe, and (d) dMn in Surface Atlantic Mixed Water (AMW) and Surface Polar Mixed Water (PMW) against *N** values.

4.2.2 River runoff

The meteoric water fractions included river runoff and local precipitation. The former dominates the signals of the Fe and Mn sources in Arctic surface waters (Dai and Martin, 1995; Guieu et al., 1996; Pokrovsky et al., 2016; Savenko and Pokrovsky, 2019). Although there was no clear relationship among f_{mw}, TdFe, and TdMn in the surface waters (Fig. S7), the dissolved fractions of metals exhibited distinct characteristics. The dFe concentrations in PMW and AMW were positively correlated with f_{mw} (Fig. 8a), suggesting that river runoff is an important factor controlling dFe concentrations in surface waters. Three large Siberian rivers, the Lena, Kolyma, and Indigirka (Fig. 1a), discharge into the LESS, likely affecting dFe concentrations in the surface waters. Moreover, the Ob and Yenisei Rivers flow into the northwestern Laptev Sea via eastward coastal currents (Bauch et al., 2011, 2014). The contribution of river water flowing into the Chukchi Sea (e.g., Yukon River) is already included within the Pacific-sourced water assignment based on water mass calculations. Thus, the variation in f_{mw} in the PMW is mainly attributed to input from Siberian rivers. At the same f_{mw} level of approximately 10%, AMW had a higher dFe relative to PMW. This could indicate that the river sources contributing to AMW had a relatively higher dFe endmember, or that some dFe in PMW underwent more removal processes than AMW. In contrast to dFe, the dMn concentrations in PMW and AMW did not correlate to f_{mw}, individually (Fig. 8b). However, if we combined AMW with PMW in all water samples and considered outliers for samples that were largely influenced by sedimentary input (Sts. 86 and 89, Fig. 1b), the dMn concentrations in the water

were positively correlated with f_{mw} (r = 0.70; p < 0.001; Fig. 8b). Consequently, dMn exhibited characteristics that differed from those of dFe.

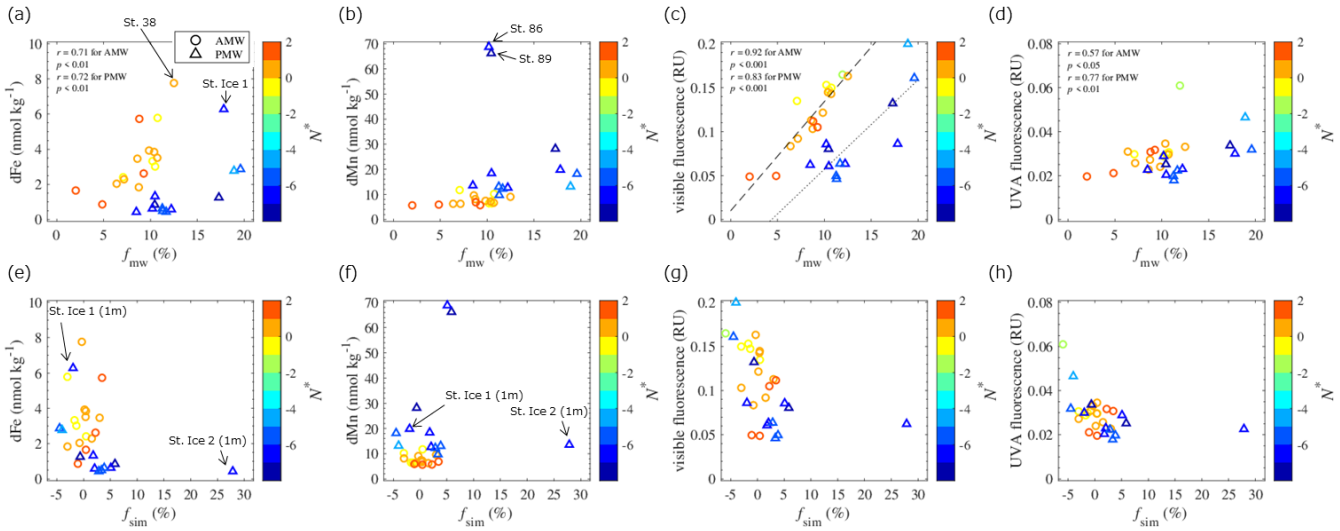

Figure 8 Plots of dFe, dMn, visible fluorescence, and UVA fluorescence in Surface Atlantic Mixed Water (AMW) and Surface Polar Mixed Water (PMW) against fractional meteoric water (f_{mw}) in (a)−(d) and sea ice meltwater (f_{sim}) in (e)−(h). The color scale shows the N* values of each water sample. Linear relationships were evaluated based on Pearson correlation coefficients (r). The liner fits of the visible fluorescence-f_{mw} relationships in the AMW and PMW are shown by dashed and dotted lines in (c), respectively.

Both metals are not equally preserved in seawater after being released from river water owing to differences in their removal kinetics. We examined the salinity-dMn/dFe ratio relationships among specific waters in LESS (Fig. 9). Data from the Yenisei River and the estuarine waters are presented for comparison. In the Lena and Yenisei estuaries, the dMn/dFe ratios increased with increasing salinity because of the preferential loss of dFe relative to dMn after release from these rivers (Fig. 9). The dMn/dFe ratios in the AMW, as well as the surface water in the Laptev Shelf/Slope, were plotted around a mixing line of freshwater (rivers) and seawater (estuaries) (Fig. 9b). On the other hand, the dMn/dFe ratio in PMW extremely deviated from the freshwater-seawater line (Fig. 9a). This was due to the intrusion of shelf-derived water with excess dMn relative to dFe into the eastern part of the LESS, as discussed in Sect. 4.2.1. Thus, the dMn distribution was driven by inputs from both shelf sediments and riverine fluxes, particularly in the PMW.

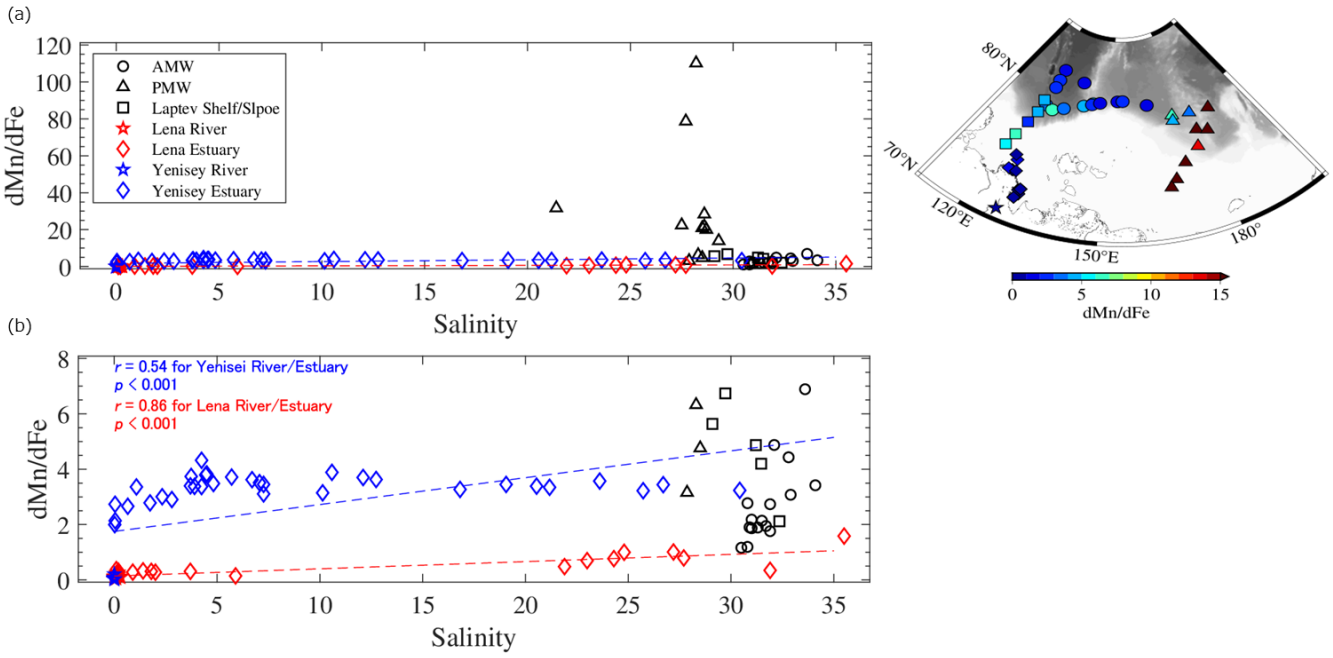

Figure 9 (a) Relationships between salinity and dFe/dMn ratio in specific water mass. A smaller scale of the Y-axis is shown in (b). The geographical distribution of each sample is indicated by different symbols as shown in the map. Mixing lines of freshwater (Lena and Yenisei rivers) and seawater (Lena and Yenisei estuaries) are derived from Hölemann et al. (2005), Peterson et al. (2016), and Savenko and Pokrovsky (2019). Linear relationships were evaluated against the freshwater-seawater line based on Pearson correlation coefficients (r). The value for surface water on the Laptev Shelf/Slope (Klunder et al., 2012; Middag et al., 2011) is plotted for comparison.

4.2.3 Sea ice formation and melt

The fraction of sea-ice meltwater includes brine drainage ($f_{sim} < 0$) or meltwater input ($f_{sim} > 0$) associated with sea-ice formation or melting. The f_{sim} values in the PMW and AMW did not correlate with any metal concentration (Figs. 8e–f and S7). The f_{sim} in the under-ice water at St. Ice 1, where we collected the ice core for trace metal analysis, showed a negative value of −2.0% (Fig. 8e−f), such that the water had received brine from the overlying sea ice. Indeed, the ice sample from St. Ice 1 was effectively permeable because the ice temperature was approximately −2℃ through the ice core with a bulk salinity of 2 (NABOS 2021 cruise report, https://uaf-iarc.org/nabos-products/). For temperatures warmer than −5℃, brine-loading dissolved fractions of trace metals, as well as heat and nutrients, can move through the ice and finally be released to the water column (Golden et al., 1998; Lannuzel et al., 2008; van der Merwe et al., 2011). Given 2% of brine inclusion in the under ice-water at St. Ice 1, the added dFe and dMn into the water column associated with brine drainage account for 0.12 nmol kg^{-1} and 0.39 nmol kg^{-1}, respectively. The same calculation for the TdFe and TdMn showed 1.3 nM and 0.45 nM, respectively.

The metal inputs throughout the brine drainage were considered low compared to other sources of Fe and Mn in the studied region.

In contrast to St. Ice 1, the under-ice water at St. Ice 2 was largely influenced by sea-ice melt, with f_{sim} as high as 27.9% at a depth of 1 m (Fig. 8e–f). The inventories of dFe and dMn over the depths of 1−10 m at St. 2 were computed as 4.5 μmol m^{-2} and 115 μmol m^{-2}, respectively. The same calculation for the TdFe and TdMn showed 9.7 μmol m^{-2} and 128 μmol m^{-2}, respectively. The inventories of under-ice water were higher than those of the ice cores collected in this study (Table 3), suggesting that sea-ice melt is not the only source of these metals in under-ice water. It should be noted that this study did not resolve the temporal evolution of sea ice melt; thus, we did not capture Fe and Mn concentrations in the sea ice at the early stages of sea ice melt. A time-series experiment conducted in Antarctic pack ice demonstrated that 70% of the Fe in sea ice was released into the under-ice water during the first 10 days of the survey, while ice cover was still present (Lannuzel et al., 2008). The lack of time-series observations in this study may result in an underestimation of the inventories of metals in sea ice. Nevertheless, sea ice formation and/or melting were less important to the overall distribution of Fe and Mn in surface LESS during the study period, although the process had a potentially local impact on the Fe and Mn cycles.

An important conclusion in this section is that the major factors controlling Fe and Mn concentrations in LESS were river discharge and shelf sediment-water exchange processes. DOM is also sourced from rivers and seafloor sediments, which are linked to the biogeochemical cycles of Fe and Mn in the Arctic (e.g., Charette et al., 2020). In the following section, we discuss the link between DOM and these metals in the LESS continental margins.

4.3 Characteristics and origins of DOM and its relation to trace metals

In the surface LESS, various concentrations of DOC were observed with the highest value of 146 μmol L^{-1} (Fig. 3f). Mean value of DOC (108 ± 19 μmol L^{-1}) was similar to value previously observed in the Laptev and East Siberian seas (Hölemann et al., 2021) but tended to be high compared to the Chukchi Sea (Chen et al., 2018; Jung et al., 2021; Tanaka et al., 2016). In addition to DOM release from productive shelf sediments (Cooper et al., 2005), regional DOM inputs from East Siberian rivers (Stedmon et al., 2011) and inputs of fresh plankton-derived DOM (Davis and Benner, 2007) result in surface waters of LESS with a high DOC signal. This study investigated the optical properties of CDOM, which are useful for understanding the composition and origin of the DOM in the studied region.

The DOC concentrations in the AMW and PMW were positively correlated with the absorption coefficient a_{350} and the intensities of visible fluorescence (Fig. 10a-b). This correlation implies that the factors controlling the DOC concentrations and the abundance of humic-like CDOM are similar in these surface waters. The intensities of visible fluorescence in AMW and PMW were strongly correlated with f_{mw} (Fig. 8c), suggesting the importance of riverine humic-like CDOM sources in surface waters. Interestingly, the linear fits of the visible fluorescence-f_{mw} relationships were different between AMW and PMW (Fig. 8c). This result indicates that the riverine endmembers of humic-like CDOM were different between AMW and PMW, that is, the Lena River was the riverine endmember of AMW, whereas the Indigirka and/or Kolyma rivers were the

endmembers of PMW. Microbial processing of DOM can also generate visible fluorescence (Nelson et al., 2004; Rochelle-Newall and Fisher, 2002; Yamashita and Tanoue, 2008). The low-*N** PMW must have received microbe-mediated visible fluorescence from the benthic remineralization of sinking organic matter on the productive Chukchi Shelf (Hioki et al., 2014; Yamashita et al., 2019).

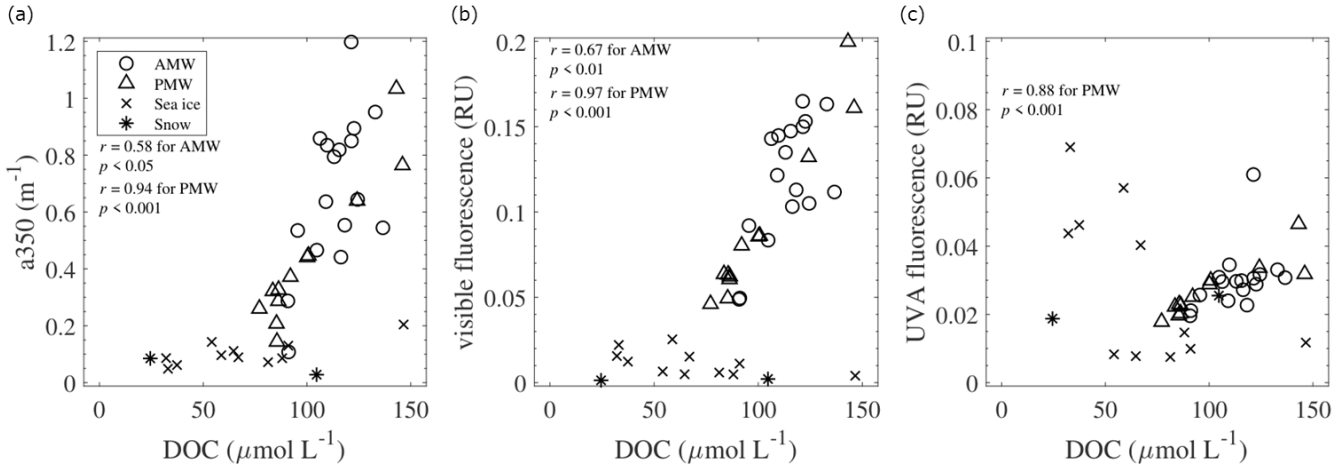

Figure 10 Relationships of DOC with (a) a_{350}, (b) visible fluorescence, and (c) UVA fluorescence in Surface Atlantic Mixed Water (AMW), Surface Polar Mixed Water (PMW), sea ice, and snow. Linear relationships were evaluated based on Pearson correlation coefficients (r).

In addition to visible fluorescence, the intensity of UVA fluorescence in PMW was positively correlated with DOC concentration; however, this does not apply to AMW (Fig. 10c). In the Arctic Ocean, UVA fluorescence is regarded as a phytoplankton-derived component (Brogi et al., 2019), including its direct release from phytoplankton and its release during grazing by zooplankton. We integrated chlorophyll fluorescence in the water column (0–10 m depth) of the PMW and compared it with the UVA fluorescence intensity (Fig. S8). The linear correlation between chlorophyll fluorescence and UVA fluorescence in PMW (r = 0.80; p < 0.01) indicates that the local production (and degradation) of UVA fluorescence is an important process. In addition, the intensity of UVA fluorescence in PMW and AMW increased with increasing f_{mw} (Fig. 8d). This result can be interpreted as the rapid transport of freshly produced labile CDOM by river water to the surface of LESS. The relationship between f_{mw} and trace metal concentrations revealed that the riverine source of dFe behaved more conservatively than that of dMn (Fig. 8a-b), which could be explained by the existence of organic ligands complexed with Fe. Previous studies on the Arctic Ocean reported that the CDOM pool contains Fe-binding organic ligands in the form of humic substances (Laglera et al., 2007, 2011; Laglera and van den Berg, 2009; Slagter et al., 2017; Williford et al., 2021). Complexes of Fe-humic substances account for approximately 80% of the dFe concentrations in the Arctic Ocean, and the concentrations of these complexes are highly correlated with the CDOM and dFe concentrations (Laglera et al., 2019). Our results show significant correlations between dFe and visible fluorescence in both AMW and PMW (Fig. 11a). The input of humic

substances from Siberian rivers into these waters was evident from the elevated intensities of visible fluorescence with f_{mw} (Fig. 8c). Thus, humic substances strongly affect the dFe concentration in seawater through complexation with Fe, which stabilizes Fe in the dissolved phase. A difference in the linear fits of dFe-visible fluorescence relationships between AMW and PMW (Fig. 11a) may be explained by the contribution of excess humic ligands from rivers to PMW. In addition to Fe, Mn is known to form organic complexes with the degradation products of organic matter, such as humic materials (e.g., Oldham et al., 2017) and biogenic siderophores (e.g., Parker et al., 2004). However, complexation of organic ligands with Mn in the Arctic Ocean is poorly understood. None of the AMW or PMW samples exhibited a significant correlation between dMn and visible fluorescence (Fig. 11b). Unlike dFe, dMn is not stabilized by humic-type organic complexes in surface waters.

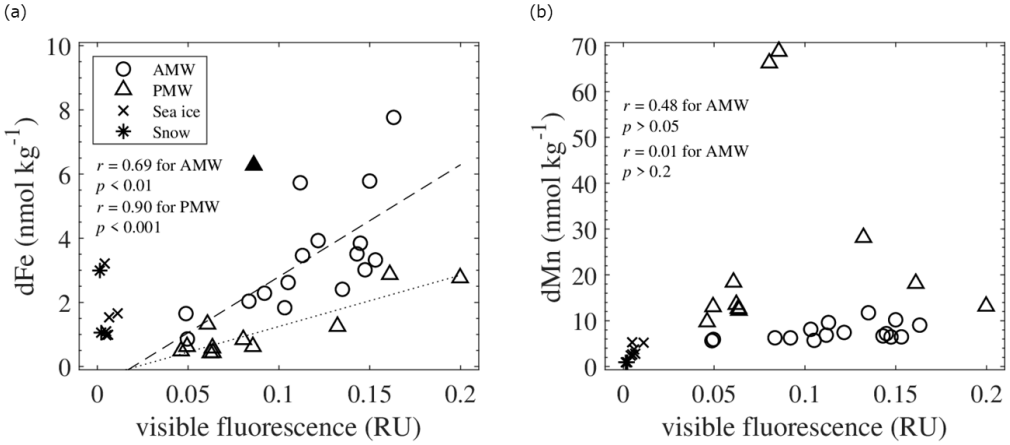

Figure 11 Relationships of visible fluorescence with (a) dFe and (b) dMn in Surface Atlantic Mixed Water (AMW), Surface Polar Mixed Water (PMW), sea ice, and snow. Linear relationships were evaluated based on Pearson correlation coefficients (r), except for an outlier (▲) in (a). The linear fits of the relationships in the AMW and PMW are shown by dashed and dotted lines in (a), respectively.

4.4 Comparison of Fe and Mn in LESS with other regions of the Arctic

To investigate the distribution patterns of dFe and dMn in the surface waters, we combined our dataset with data available for the Arctic Ocean (Cid et al., 2011, 2012; GEOTRACES Intermediate Data Product Group, 2023; Gerringa et al., 2021; Hölemann et al., 2005; Jensen et al., 2020; Klunder et al., 2012; Kondo et al., 2016; Middag et al., 2011; Rijkenberg et al., 2018; Savenko and Pokrovsky, 2019). The dFe concentrations are relatively low (up to 2 nmol kg^{-1}) in the Atlantic sectors of the Arctic Ocean (Fig. 12a). On the surfaces of the Nansen Basin and Barents Sea, Fe is expected to be the first nutrient to be depleted by primary producers (Rijkenberg et al., 2018), and phytoplankton consumption could be an important sink for Fe. In the LESS continental margins, however, surface dFe concentrations are significant (> 5 nmol kg^{-1}) and even persist in the late summer of 2021 (Fig. 12a). Figure 13a shows a boxplot of the surface dFe concentration combined with our dataset, with

the available data reported for each region in the Arctic Ocean (Fig. 13 a and c). All water samples in Figure 13 had salinity greater than 25. The result shows that the median value was the highest in Bering Sea (4.7 nmol kg^{-1}) followed by Chukchi Sea (3.1 nmol kg^{-1}) and by LESS (2.8 nmol kg^{-1}). We deduce that sedimentary Fe originating from the reductive Bering Shelf was gradually removed from the Chukchi Sea after entering it from the Bering Strait (Jansen et al., 2020), and then penetrated the East Siberian Sea. The dFe concentrations also increased in the estuaries of the Lena, Yenisei, and Mackenzie Rivers (Fig. 12a). Other studies determined that dFe concentration in the estuary water (salinity < 25) of the Lena River was as high as 9,000 nmol kg^{-1}, as well as in the estuary waters of the Yenisei and Mackenzie rivers. Fe-binding organic ligands in the form of humic substances originating from the Lena River strongly affect the dFe concentration, as discussed in the previous section. The natural humic substance Fe ligands of the Arctic Ocean surface belong to a group of strong ligands ubiquitous in surface ocean waters (Laglera et al., 2019). Strongly complexed Fe may be less biologically available to the phytoplankton community than weakly complexed Fe released from grazing and bacterial remineralization of organic matter (Gledhill and Buck, 2012). The river-influenced water from the LESS continental margins is the source water of the Trans Polar Drift, which enriches dFe in the Central Arctic Ocean (Fig. 12a) (Charette et al., 2020; Gerringa et al., 2021; Klunder et al., 2012).

The high dMn found in the Central Arctic Ocean (Fig. 12b) was also related to the presence of Trans Polar Drift (Charette et al., 2020; Gerringa et al., 2021). In addition to riverine inputs, sediment-water column exchange over shelves leads to relatively dMn-rich water in the Pacific sector of the Arctic Ocean. The dMn concentrations increased toward the broad shelves of the East Siberian Sea (~68 nmol kg^{-1}), Chukchi Sea (~45 nmol kg^{-1}), and Bering Sea (~103 nmol kg^{-1}), whereas the concentration was relatively low (~8 nmol kg^{-1}) over a narrow shelf of Beaufort Sea (Fig. 12b). Boxplot of the surface dMn concentration in Fig. 13b shows that the difference of median value is relatively small among LESS (13.0 nmol kg^{-1}), Chukchi Sea (12.4 nmol kg^{-1}), and Bering Sea (12.2 nmol kg^{-1}). As previously discussed, the shelf sediment-water exchange processes over the Chukchi Shelf largely influence the Fe and Mn distributions in the East Siberian Sea. Vieira et al. (2019) provided the first estimate of the benthic flux of the radium isotope (Ra^{228}) in the Chukchi Sea as a tracer of benthic trace metal inputs, which was among the highest rates reported globally. The low-N^* water spread over regions where nitrate was already depleted relative to phosphate, mainly because of the oxidation of organic matter by bacteria in the reductive shelf sediment (Fig. 12c). The East Siberian Sea and the Chukchi Sea are likely hotspots of sediment-sourced dMn via the reductive dissolution of Mn oxide in the sediment. A multistep removal process of dMn has been suggested in the Arctic (Jansen et al., 2020): dMn is rapidly removed to the particulate phase within 150 km of the shelf break, but some dMn remains conserved throughout the next 1000 km away from the shelf. The dMn originating from the LESS continental margins appears to be effectively exported by the Trans Polar Drift to the Central Arctic Ocean (Fig. 12b), although stabilization by organic complexation is unlikely for Mn during offshore transport.

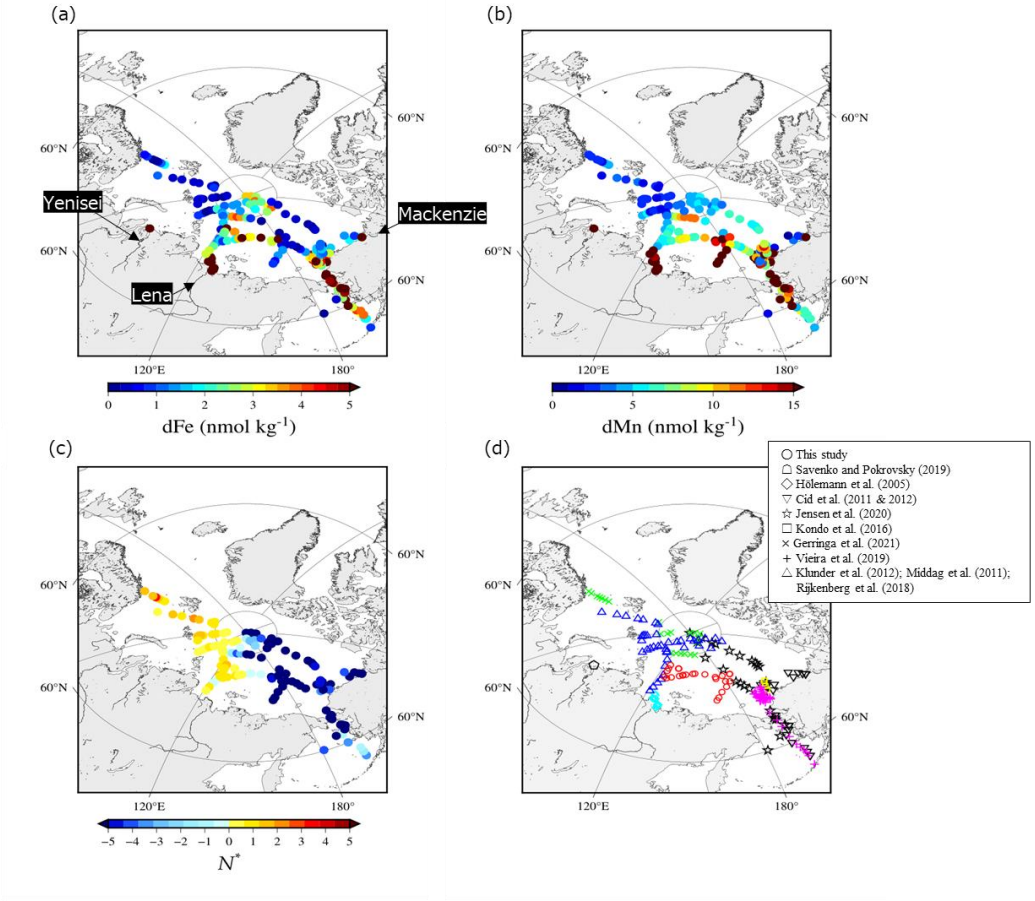

495

Figure 12 Spatial distributions in (a) dFe, (b) dMn, and (c) *N** in surface water (< 25 m depth) in the Arctic Ocean. (d) Location of stations on dFe, dMn, and *N** reported by this study and the previous studies.

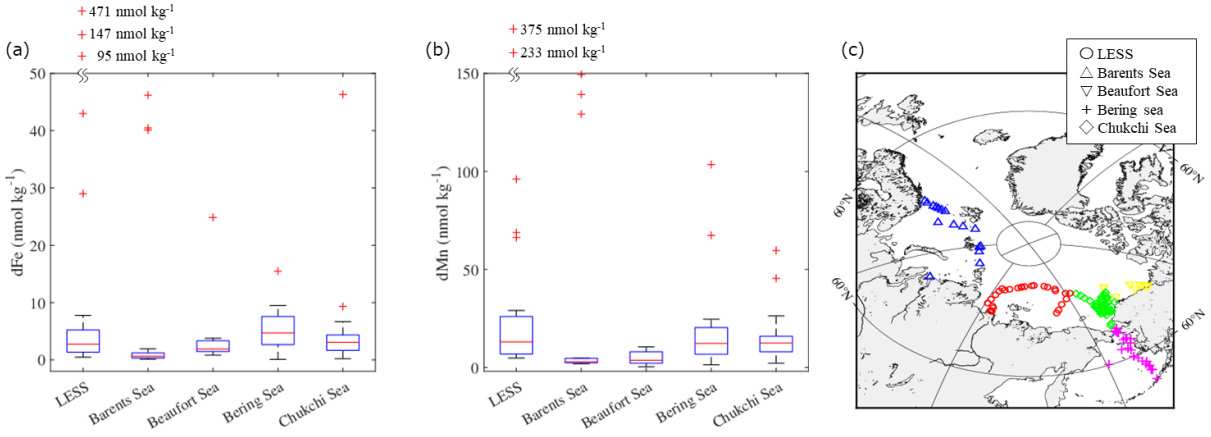

Figure 13 Boxplots of (a) dFe and (b) dMn concentrations in surface water (< 25 m depth) in each region of the Arctic Ocean. (c) Location of stations used in this boxplot. The bottom and top of the box in (a)–(b) indicate the 25th and 75th percentiles, respectively, and the line inside the box indicates the median. The bottom and top error bars in (a)–(b) show minimum and maximum values, respectively, and the outliers are plotted individually using the '+' marker symbol. Some outliers are plotted on the outside of figures to better represent the differences between the regions.

5 Conclusion

Our results indicate that two governing hydrographic regimes exist in the surface waters of the LESS continental margins in the late summer of 2021. The East Siberian Sea and Chukchi Abyssal Plain are dominated by Pacific-sourced water, whereas the Makarov and Amundsen basins are dominated by the intrusion of Atlantic-sourced water, which is in agreement with previous studies (e.g., Bauch et al., 2011). In these regions, the impact of river water discharge on the chemical properties of the surface water is significant. However, sea-ice melting/formation was less important during our observations. A positive correlation between the f_{mw}, dFe, and humic-like CDOM in the LESS site confirmed a common freshwater source for dFe and humic-like CDOM. Humic-like organic ligands likely stabilized Fe in the dissolved phase, which was not the case for Mn. The East Siberian Sea and Chukchi Abyssal Plain are characterized by particularly low-N^* values, resulting from a large sedimentary flux that releases Mn over the continental shelf. The LESS is a key region originating from large amounts of shelf-derived nutrients, organic carbon, and trace elements (Charette et al., 2020; Jensen et al., 2021; Kipp et al., 2018). Shelf-derived materials and materials from riverine sources are transported to the Central Arctic via the Trans Polar rift. Changes in the LESS region may affect the magnitude of material flux to the remote open ocean. This effect likely has a major impact on primary production and species composition in the Arctic surface waters. Further investigations in LESS are required to elucidate how shelf- and river-derived elements are mixed within the water column and transported off-shelf.

Acknowledgments

This expedition was supported by the ArCSII (JPMXD1420318865) International Exchange Program "Arctic Ocean: Improving tools and information for northern populations and safe navigation" and was coordinated by T. Alekseeva of AARI, Russia. We thank the members of the 2021 NABOS expedition. We are grateful to K. Kurashima and S. Otosaka for their assistance with the laboratory work. This research was funded by the Japanese Ministry of Education, Culture, Sports, Science and Technology through JSPS KAKENHI (20J01213, 20K19949 and 23K17028). This research was also supported by a Grant for the Joint Research Program of the Japan Arctic Research Network Center and by the Research Institute for Oceanochemistry Foundation.

Code/Data availability Data are available upon request from the corresponding author (N. Kanna).

Author contributions: N. Kanna and H. Obata designed this study. I. Polyakov and T. Waseda supervised the NABOS expedition. N. Kanna, K. Tateyama, A. Timofeeva, M. Papadimitraki, and L. Whitmore carried out the sampling, and N. Kanna analyzed the samples. D. Nomura, H. Ogawa, and Y. Yamashita supervised the $\delta^{18}O$, nutrients, and DOM analyses. All the authors contributed to the manuscript.

Competing interests: The authors declare that they have no competing interests.

References

Aguilar-Islas, A.M., Rember, R., Nishino, S., Kikuchi, T., and Itoh, M.: Partitioning and lateral transport of iron to the Canada Basin, Polar Sci. 7, 82–99, 2013.

Alling, V., Sanchez-garcia, L., Porcelli, D., Pugach, S., Vonk, J.E., Van Dongen, B., Mörth, C., Anderson, L.G., Sokolov, A., Andersson, P., Humborg, C., Semiletov, I., and Gustafsson, Ö.: Nonconservative behavior of dissolved organic carbon across the Laptev and East Siberian seas, Global Biogeochem. Cycles 24, 2010.

Anderson, L. G. and Macdonald R. W.: Observing the Arctic Ocean carbon cycle in a changing environment, Polar Res. 34. https://doi.org/10.3402/polar.v34.26891, 2015.

Anderson, L.G., Björk, G., Holby, O., Jutterström, S., Mörth, C.M., O'Regan, M., Pearce, C., Semiletov, I., Stranne, C., and Stöven, T.: Shelf–basin interaction along the East Siberian Sea, Ocean Sci. 13, 349–363, 2017.

Bauch, D., Van Der Loeff, M.R., Andersen, N., Torres-Valdes, S., Bakker, K., and Abrahamsen, E.P.: Origin of freshwater and polynya water in the Arctic Ocean halocline in summer 2007. Prog. Oceanogr. 91, 482, 2011.

Bauch, D., Torres-Valdes, S., Polyakov, I., Novikhin, A., Dmitrenko, I., McKay, J., and Mix, A.: Halocline water modification and along-slope advection at the Laptev Sea continental margin, Ocean Sci., 10(1), 141–154, 2014.

Bauch, D., and Cherniavskaia, E.: Water mass classification on a highly variable arctic shelf region: Origin of Laptev sea water masses and implications for the nutrient budget, J. Geophys. Res. Oceans 123(3), 1896–1906, 2018.

Brogi, S., Jung, J.Y., Ha, S., and Hur, J.: Seasonal differences in dissolved organic matter properties and sources in an Arctic fjord: Implications for future conditions, Sci Total Environ. 694, 2019.

Bolt, C., Aguilar-Islas, A., and Rember, R.: Particulate trace metals in Arctic snow, sea ice, and underlying surface waters during the 2015 US western Arctic GEOTRACES cruise GN01, ACS Earth Space Chem. 4, 2444–2460, 2020.

Charette, M.A., Kipp, L.E., Jensen, L.T., Dabrowski, J.S., Whitmore, L.M., Fitzsimmons, J.N., Williford, T., Ulfsbo, A., Jones, E., Bundy, R.M., Vivancos, S.M., Pahnke, K., John, S.G., Xiang, Y., Hatta, M., Petrova, M.V., Heimbürger-Boavida, L., Bauch, D., Newton, R., Pasqualini, A., Agather, A.M., Amon, R.M.W., Anderson, R.F., Andersson, P.S., Benner, R., Bowman, K.L., Edwards, R.L., Gdaniec, S., Gerringa, L.J.A., González, A.G., Granskog, M., Haley, B., Hammerschmidt, C.R., Hansell, D.A., Henderson, P.B., Kadko, D.C., Kaiser, K., Laan, P., Lam, P.J., Lamborg, C.H., Levier, M., Li, X., Margolin, A.R., Measures, C., Middag, R., Millero, F.J., Moore, W.S., Paffrath, R., Planquette, H., Rabe, B., Reader, H., Rember, R.,

Rijkenberg, M.J.A., Roy-Barman, M., Rutgers van der Loeff, M., Saito, M., Schauer, U., Schlosser, P., Sherrell, R.M., Shiller, A.M., Slagter, H., Sonke, J.E., Stedmon, C., Woosley, R.J., Valk, O., van Ooijen, J., and Zhang, R.: The transpolar drift as a source of riverine and shelf-derived trace elements to the Central Arctic Ocean, J. Geophys. Res. Oceans e2019JC015920, 2020.

Chen, M., Jung, J., Lee, Y.K., and Hur, J.: Surface accumulation of low molecular weight dissolved organic matter in surface waters and horizontal off-shelf spreading of nutrients and humic-like fluorescence in the Chukchi Sea of the Arctic Ocean, Sci. Total Environ. 639, 624, 2018.

Cid, A.P., Urushihara, S., Minami, T., Norisuye, K., and Sohrin, Y.: Stoichiometry among bioactive trace metals in seawater on the Bering Sea shelf, J. Oceanogr. 67, 747, 2011.

Cid, A.P., Nakatsuka, S., and Sohrin, Y.: Stoichiometry among bioactive trace metals in the Chukchi and Beaufort Seas, J. Oceanogr. 68, 985, 2012.

Clement Kinney, J., Assmann, K.M., Maslowski, W., Björk, G., Jakobsson, M., Jutterström, S., Lee, Y.J., Osinski, R., Semiletov, I., Ulfsbo, A.: On the circulation, water mass distribution, and nutrient concentrations of the western Chukchi Sea, Ocean Sci. 18, 29–49, 2022.

Coble, P.G.: Characterization of marine and terrestrial DOM in seawater using excitation-emission matrix spectroscopy, Mar. Chem. 51, 325–346, 1996.

Cooper, L.W., Benner, R., Mcclelland, J.W., Peterson, B.J., Holmes, R.M., Raymond, P.A., Hansell, D.A., Grebmeier, J.M., and Codispoti, L.A.: Linkages among runoff, dissolved organic carbon, and the stable oxygen isotope composition of seawater and other water mass indicators in the Arctic Ocean, J. Geophys. Res. 110, 2005.

Dai, M., and Martin, J.: First data on trace metal level and behavior in two major Arctic river-estuarine systems (Ob and Yenisey) and in the adjacent Kara Sea, Russia, Earth Planet. Sci. Lett. 131, 127–141, 1995.

Davis, J. and Benner, R.: Quantitative estimates of labile and semi-labile dissolved organic carbon in the Western Arctic Ocean: A molecular approach, Limnol. Oceanogr. 52, 2434–2444, 2007.

Doglioni, F., Ricker, R., Rabe, B., Barth, A., Troupin, C., and Kanzow, T.: Sea surface height anomaly and geostrophic current velocity from altimetry measurements over the Arctic Ocean (2011–2020), Earth Syst. Sci. Data Discuss. 2022, 1–51, 2022.

Evans, L.K. and Nishioka, J.: Accumulation processes of trace metals into Arctic sea ice: distribution of Fe, Mn and Cd associated with ice structure, Mar. Chem. 209, 36-47, 2019.

Eicken, H., Kolatschek, J., Freitag, J., Lindemann, F., Kassens, H., and Dmitrenko, I.: A key source area and constraints on entrainment for basin-scale sediment transport by Arctic sea ice, Geophys. Res. Lett. 27, 1919–1922, 2000.

Feng, D., Gleason, C.J., Lin, P., Yang, X., Pan, M., and Ishitsuka, Y.: Recent changes to Arctic river discharge, Nat. Commun. 12, 6917, 2021.

Fox-Kemper, B., H.T. Hewitt, C. Xiao, G. Aðalgeirsdóttir, S.S. Drijfhout, T.L. Edwards, N.R. Golledge, M. Hemer, R.E. Kopp, G. Krinner, A. Mix, D. Notz, S. Nowicki, I.S. Nurhati, L. Ruiz, J.-B. Sallée, A.B.A. Slangen, and Y. Yu.: Ocean, cryosphere

and sea Level Change. In Climate Change 2021: The Physical Science Basis. Contribution of Working Group I to the Sixth Assessment Report of the Intergovernmental Panel on Climate Change [Masson-Delmotte, V., P. Zhai, A. Pirani, S.L. Connors, C. Péan, S. Berger, N. Caud, Y. Chen, L. Goldfarb, M.I. Gomis, M. Huang, K. Leitzell, E. Lonnoy, J.B.R. Matthews, T.K. Maycock, T. Waterfield, O. Yelekçi, R. Yu, and B. Zhou (eds.)].: Cambridge University Press, Cambridge, United Kingdom and New York, NY, USA, pp. 1211–1362, doi: 10.1017/9781009157896.011, 2021.

GEOTRACES Intermediate Data Product Group: The GEOTRACES Intermediate Data Product 2021v2 (IDP2021v2). NERC EDS British Oceanographic Data Centre NOC. doi:10.5285/ff46f034-f47c-05f9-e053-6c86abc0dc7e, 2023

Gerringa, L.J.A., Rijkenberg, M.J.A., Slagter, H.A., Laan, P., Paffrath, R., Bauch, D., Rutgers Van Der Loeff, M., and Middag, R.: Dissolved Cd, Co, Cu, Fe, Mn, Ni, and Zn in the Arctic Ocean, JGR Oceans 126, 2021.

Gledhill, M., and Buck, K.N.: The organic complexation of iron in the marine environment: a review, Front. Microbiol. 3, 18807, 2012.

Golden, K.M., Ackley, S.F., and Lytle, V.I.: The percolation phase transition in sea ice, Science 282, 2238–2241, 1998

Goto, S., Tada, Y., Suzuki, K., and Yamashita, Y.: Evaluation of the Production of Dissolved Organic Matter by Three Marine Bacterial Strains, Front. Microbiol. 11, 584419, 2020.

Green, S.A. and Blough, N.V.: Optical absorption and fluorescence properties of chromophoric dissolved organic matter in natural waters, Limnol. Oceanogr. 39, 1903–1916, 1994.

Gruber, N. and Sarmiento, J.L.: Global patterns of marine nitrogen fixation and denitrification, Global Biogeochem. Cycles 11, 235–266, 1997.

Guieu, C., Huang, W.W., Martin, J., and Yong, Y.Y.: Outflow of trace metals into the Laptev Sea by the Lena River, Mar. Chem. 53, 255–267, 1996.

Hioki, N., Kuma, K., Morita, Y., Sasayama, R., Ooki, A., Kondo, Y., Obata, H., Nishioka, J., Yamashita, Y., Nishino, S., and Kikuchi, T.: Laterally spreading iron, humic-like dissolved organic matter and nutrients in cold, dense subsurface water of the Arctic Ocean. Sci. Rep. 4, 6775, 2014.

Hölemann, J.A., Schirmacher, M., Kassens, H., and Prange, A.: Geochemistry of surficial and ice-rafted sediments from the Laptev Sea (Siberia), Estuar. Coast. Shelf Sci. 49, 45–59, 1999a.

Hölemann, J.A., Schirmacher, M., and Prange, A.: Dissolved and particulate major and trace elements in newly formed ice from the Laptev Sea (Transdrift III, October 1995), in: Anonymous land-ocean systems in the Siberian Arctic: Dynamics and history, Springer, pp. 101–111, 1999b.

Hölemann, J.A., Schirmacher, M., and Prange, A.: Seasonal variability of trace metals in the Lena River and the southeastern Laptev Sea: Impact of the spring freshet, Glob. Planet. Change 48, 112, 2005.

Hölemann, J.A., Juhls, B., Bauch, D., Janout, M., Koch, B.P., and Heim, B.: The impact of the freeze–melt cycle of land-fast ice on the distribution of dissolved organic matter in the Laptev and East Siberian seas (Siberian Arctic), Biogeosciences 18, 3637, 2021

Jensen, L.T., Morton, P., Twining, B.S., Heller, M.I., Hatta, M., Measures, C.I., John, S., Zhang, R., Pinedo-Gonzalez, P., Sherrell, R.M., and Fitzsimmons, J.N.: A comparison of marine Fe and Mn cycling: U.S. GEOTRACES GN01 Western Arctic case study, Geochimica et Cosmochimica Acta 288, 138, 2020.

Jensen, L.T., Lanning, N.T., Marsay, C.M., Buck, C.S., Aguilar-islas, A.M., Rember, R., Landing, W.M., Sherrell, R.M., and Fitzsimmons, J.N.: Biogeochemical cycling of colloidal trace metals in the Arctic Cryosphere, JGR Oceans 126, 2021.

Jung, J., Son, J.E., Lee, Y.K., Cho, K., Lee, Y., Yang, E.J., Kang, S., and Hur, J.: Tracing riverine dissolved organic carbon and its transport to the halocline layer in the Chukchi Sea (western Arctic Ocean) using humic-like fluorescence fingerprinting, Sci. Total Environ. 772, 2021.

Jones, E.P., Anderson, L.G., Jutterström, S., Mintrop, L., and Swift, J.H.: Pacific freshwater, river water and sea ice meltwater across Arctic Ocean basins: Results from the 2005 Beringia Expedition, J. Geophys. Res. Oceans 113, 2008.

Kadko, D., Galfond, B., Landing, W.M., and Shelley, R.U.: Determining the pathways, fate, and flux of atmospherically derived trace elements in the Arctic ocean/ice system, Mar. Chem. 182, 38–50, 2016.

Kadko, D., Aguilar-Islas, A., Bolt, C., Buck, C.S., Fitzsimmons, J.N., Jensen, L.T., Landing, W.M., Marsay, C.M., Rember, R., Shiller, A.M., Whitmore, L.M., and Anderson, R.F.: The residence times of trace elements determined in the surface Arctic Ocean during the 2015 US Arctic GEOTRACES expedition, Mar. Chem. 208, 56, 2018.

Kanna, N., Toyota, T., and Nishioka, J.: Iron and macro-nutrient concentrations in sea ice and their impact on the nutritional status of surface waters in the southern Okhotsk Sea, Progr. Oceonogr. 126, 44-57, 2014.

Kanna, N., Sugiyama, S., Ando, T., Wang, Y., Sakuragi, Y., Hazumi, T., Matsuno, K., Yamaguchi, A., Nishioka, J., Yamashita, Y.: Meltwater discharge from marine-terminating glaciers drives biogeochemical conditions in a Greenlandic fjord, Global Biogeochem. Cycles, 36, e2022GB007411, 2022

Kipp, L.E., Charette, M.A., Moore, W.S., Henderson, P.B., and Rigor, I.G.: Increased fluxes of shelf-derived materials to the central Arctic Ocean, Sci. Adv. 4, eaao1302, 2018.

Klunder, M.B., Bauch, D., Laan, P., De Baar, H.J.W., Van Heuven, S., and Ober, S.: Dissolved iron in the Arctic shelf seas and surface waters of the central Arctic Ocean: Impact of Arctic river water and ice-melt. J. Geophys. Res. 117, 2012.

Kondo, Y., Obata, H., Hioki, N., Ooki, A., Nishino, S., Kikuchi, T., and Kuma, K.: Transport of trace metals (Mn, Fe, Ni, Zn and Cd) in the Western Arctic Ocean (Chukchi sea and Canada basin) in late summer 2012, Deep-Sea Res. I: Oceanogr. Res. Pap. 116, 236–252, 2016.

Laglera, L.M., Battaglia, G., and van den Berg, C.M.: Determination of humic substances in natural waters by cathodic stripping voltammetry of their complexes with iron, Anal. Chim. Acta 599, 58–66, 2007.

Laglera, L.M., Battaglia, G., and van den Berg, C.M.: Effect of humic substances on the iron speciation in natural waters by CLE/CSV, Mar. Chem. 127, 134–143, 2011.

Laglera, L.M. and van den Berg, C.M.: Evidence for geochemical control of iron by humic substances in seawater, Limnol. Oceanogr. 54, 610–619, 2009.

Lannuzel, D., Schoemann, V., De Jong, J., Chou, L., Delille, B., Becquevort, S., and Tison, J.: Iron study during a time series in the western Weddell pack ice, Mar. Chem. 108, 85–95, 2008.

Laglera, L.M., Sukekava, C., Slagter, H.A., Downes, J., Aparicio-Gonzalez, A., and Gerringa, L.J.A.: First quantification of the controlling role of humic substances in the transport of iron across the surface of the Arctic Ocean, Environ. Sci. Technol. 53, 13136, 2019.

Lewis, K.M., van Dijken, G.L., and Arrigo, K.R.: Changes in phytoplankton concentration now drive increased Arctic Ocean primary production, Science (American Association for the Advancement of Science) 369, 198–202, 2020.

Landing, W.M. and Bruland, K.W.: The contrasting biogeochemistry of iron and manganese in the Pacific Ocean, Geochim. Cosmochim. Acta 51, 29–43, 1987.

Lannuzel, D., Schoemann, V., de Jong, J., Chou, L., Delille, B., Becquevort, S., and Tison, J.: Iron study during a time series in the western Weddell pack ice, Mar. Chem. 108, 85–95, 2008.

Lawaetz, A. J., and Stedmon, C. A.: Fluorescence intensity calibration using the Raman scatter peak of water, Applied spectroscopy, 63(8), 936–940, 2009.

Marsay, C. M., Kadko, D., Landing, W. M., Morton, P. L., Summers, B. A., and Buck, C. S.: Concentrations, provenance and flux of aerosol trace elements during US GEOTRACES Western Arctic cruise GN01, Chem. Geol. 502, 1–14, 2018.

Measures, C.I.: The role of entrained sediments in sea ice in the distribution of aluminium and iron in the surface waters of the Arctic Ocean, Mar. Chem. 68, 59–70, 1999.

Middag, R., De Baar, H.J.W., Laan, P., and Klunder, M.B.: Fluvial and hydrothermal input of manganese into the Arctic Ocean, Geochim. Cosmochim. Acta 75, 2393, 2011.

Millero, F.J., Sotolongo, S., and Izaguirre, M.: The oxidation kinetics of Fe(II) in seawater, Geochim. Cosmochim. Acta 51, 793-801, 1987.

Morel, F.M. and Price, N.M.: The biogeochemical cycles of trace metals in the oceans, Science 300, 944–947, 2003.

Nakayama, Y., Fujita, S., Kuma, K., and Shimada, K.: Iron and humic-type fluorescent dissolved organic matter in the Chukchi Sea and Canada Basin of the western Arctic Ocean. J. Geophys. Res. Oceans 116, 2011.

Nelson, N.B., Carlson, C.A., and Steinberg, D.K.: Production of chromophoric dissolved organic matter by Sargasso Sea microbes, Mar. Chem. 89, 273–287, 2004.

Newton, R., Schlosser, P., Mortlock, R., Swift, J., and Macdonald, R.: Canadian Basin freshwater sources and changes: Results from the 2005 Arctic Ocean Section, J. Geophys. Res. Oceans 118, 2133, 2013.

Nishimura, S., Kuma, K., Ishikawa, S., Omata, A., and Saitoh, S.: Iron, nutrients, and humic-type fluorescent dissolved organic matter in the northern Bering Sea shelf, Bering Strait, and Chukchi Sea, J. Geophys. Res. Oceans 117, 2012.

Nishino, S., Itoh, M., Williams, W.J., and Semiletov, I.: Shoaling of the nutricline with an increase in near-freezing temperature water in the Makarov Basin, J. Geophys. Res. Oceans 118, 635, 2013

Oldham, J. and Tebo, L.: Oxidative and reductive processes contributing to manganese cycling at oxic-anoxic interfaces, Mar. Chem. 195, 122–128, 2017.

Parker, D.L., Sposito, G., and Tebo, B.M.: Manganese (III) binding to a pyoverdine siderophore produced by a manganese (II)-oxidizing bacterium, Geochim. Cosmochim. Acta 68, 4809–4820, 2004.

Peterson, B.J, Holmes, R.M, McClelland, J.W., Amon, R., Brabets, T., Cooper, L., Gibson, John., Gordeev, V.V., Guay, C., Milburn, D., Staples, R., Raymond, I P.A., Shiklomanov, G., Striegl, R. G., Zhulidov, A., Gurtovaya, T., Sergey, Z.: PARTNERS Project Arctic River Biogeochemical Data, Arctic Data Center. doi:10.18739/A2HD33.

Pokrovsky, O.S., Manasypov, R.M., Loiko, S.V., Krickov, I.A., Kopysov, S.G., Kolesnichenko, L.G., Vorobyev, S.N., and Kirpotin, S.N., 2016.: Trace element transport in western Siberian rivers across a permafrost gradient, Biogeosciences 13, 1877–1900, 2016.

Polyakov, I.V., Ingvaldsen, R.B., Pnyushkov, A.V., Bhatt, U.S., Francis, J.A., Janout, M., Kwok, R., Skagseth, Ø.: Fluctuating Atlantic inflows modulate Arctic atlantification, Science (American Association for the Advancement of Science) 381, 972–979, 2023

Polyakov, I.V., Pnyushkov, A.V., Alkire, M.B., Ashik, I.M., Baumann, T.M., Carmack, E.C., Goszczko, I., Guthrie, J., Ivanov, V.V., Kanzow, T., Krishfield, R., Kwok, R., Sundfjord, A., Morison, J., Rember, R., Yulin, A.:. Greater role for Atlantic inflows on sea-ice loss in the Eurasian Basin of the Arctic Ocean. Science (American Association for the Advancement of Science) 356, 285–291, 2017

Polyakov, I.V., Alkire, M.B., Bluhm, B.A., Brown, K.A., Carmack, E.C., Chierici, M., Danielson, S.L., Ellingsen, I., Ershova, E.A., Gårdfeldt, K., Ingvaldsen, R.B., Pnyushkov, A.V., Slagstad, D., Wassmann, P.: Borealization of the Arctic Ocean in Response to Anomalous Advection From Sub-Arctic Seas, Front. Mar. Sci. 7, 2020

Rantanen, M., Karpechko, A.Y., Lipponen, A., Nordling, K., Hyvärinen, O., Ruosteenoja, K., Vihma, T., and Laaksonen, A.: The Arctic has warmed nearly four times faster than the globe since 1979, Commun. Earth. Environ. 3, 2022.

Rijkenberg, M.J.A., Slagter, H.A., Rutgers van der Loeff, M., van Ooijen, J., and Gerringa, L.J.A: Dissolved Fe in the Deep and Upper Arctic Ocean With a Focus on Fe Limitation in the Nansen Basin, Front. Mar. Sci. 5:88, 2018.

Rochelle-Newall, E.J., and Fisher, T.R.: Production of chromophoric dissolved organic matter fluorescence in marine and estuarine environments: an investigation into the role of phytoplankton, Mar. Chem. 77, 7–21, 2002.

Rogalla, B., Allen, S.E., Colombo, M., Myers, P.G., and Orians, K.J.: Sediments in sea ice drive the Canada Basin surface Mn maximum: insights from an Arctic Mn ocean model, Global Biogeochem. Cycles 36, e2022GB007320, 2022.

Rudels, B., Jones, E.P., Schauer, U., and Eriksson, P.: Atlantic sources of the Arctic Ocean surface and halocline waters, Polar Res. 23, 181–208, 2004.

Savenko, A.V., Pokrovsky, O.S.: Distribution of dissolved matter in the Yenisei estuary and adjacent Kara Sea areas and its inter-annual variability, Geochem. Int. 57, 1201–1212, 2019.

Shiozaki, T., Fujiwara, A., Ijichi, M., Harada, N., Nishino, S., Nishi, S., Nagata, T., and Hamasaki, K.: Diazotroph community structure and the role of nitrogen fixation in the nitrogen cycle in the Chukchi Sea (western Arctic Ocean), Limnol. Oceanogr. 63, 2191, 2018.

Slagter, H.A., Reader, H.E., Rijkenberg, M.J.A., Rutgers Van Der Loeff, M., De Baar, H.J.W., and Gerringa, L.J.A.: Organic Fe speciation in the Eurasian Basins of the Arctic Ocean and its relation to terrestrial DOM. Mar. Chem. 197, 11, 2017.

Sohrin, Y., Urushihara, S., Nakatsuka, S., Kono, T., Higo, E., Minami, T., Norisuye, K., and Umetani, S.: Multielemental determination of GEOTRACES key trace metals in seawater by ICPMS after preconcentration using an ethylenediaminetriacetic Acid Chelating Resin, Anal. Chem. (Washington) 80, 6267–6273, 2008.

Stabeno, P., Kachel, N., Ladd, C., and Woodgate, R.: Flow patterns in the eastern Chukchi Sea: 2010–2015, J. Geophys. Res. Oceans 123, 1177–1195, 2018.

Stedmon, C.A. and Bro, R.: Characterizing dissolved organic matter fluorescence with parallel factor analysis: a tutorial, Limnol. Oceanogr. Methods 6, 572–579, 2008.

Stedmon, C.A., Amon, R., Rinehart, A.J., and Walker, S.A.: The supply and characteristics of colored dissolved organic matter (CDOM) in the Arctic Ocean: Pan Arctic trends and differences, Mar. Chem. 124, 108–118, 2011.

Sumata, H., De Steur, L., Divine, D.V., Granskog, M.A., and Gerland, S.: Regime shift in Arctic Ocean sea ice thickness, Nature 615, 443, 2023.

Tanaka, K., Takesue, N., Nishioka, J., Kondo, Y., Ooki, A., Kuma, K., Hirawake, T., and Yamashita, Y.: The conservative behavior of dissolved organic carbon in surface waters of the southern Chukchi Sea, Arctic Ocean, during early summer, Sci. Rep. 6, 2016.

Tovar-Sánchez, A., Duarte, C.M., Alonso, J.C., Lacorte, S., Tauler, R., and Galbán-Malagón, C.: Impacts of metals and nutrients released from melting multiyear Arctic sea ice, J. Geophys. Res. Oceans 115, 2010.

Twining, B.S. and Baines, S.B.: The Trace Metal Composition of Marine Phytoplankton. Annu. Rev. Mar. Sci. 5, 191-215.

Van der Merwe, P., Lannuzel, D., Bowie, A.R., and Meiners, K.M.: High temporal resolution observations of spring fast ice melt and seawater iron enrichment in East Antarctica, J. Geophys. Res. Biogeosciences 116, 2011.

Vieira, L.H., Achterberg, E.P., Scholten, J., Beck, A.J., Liebetrau, V., Mills, M.M., and Arrigo, K.R.: Benthic fluxes of trace metals in the Chukchi Sea and their transport into the Arctic Ocean, Mar. Chem. 208, 43, 2018.

Waga, H., Eicken, H., Light, B., and Fukamachi, Y.: A neural network-based method for satellite-based mapping of sediment-laden sea ice in the Arctic, Remote Sens. Environ. 270, 112861, 2022.

Wegner, C., Wittbrodt, K., Hölemann, J.A., Janout, M.A., Krumpen, T., Selyuzhenok, V., Novikhin, A., Polyakova, Y., Krykova, I. and Kassens, H.: Sediment entrainment into sea ice and transport in the Transpolar Drift: A case study from the Laptev Sea in winter 2011/2012, Cont. Shelf Res. 141, 1–10, 2017

Williford, T., Amon, R.M.W., Benner, R., Kaiser, K., Bauch, D., Stedmon, C., Yan, G., Walker, S.A., Van Der Loeff, M.R., and Klunder, M.B.: Insights into the origins, molecular characteristics and distribution of iron-binding ligands in the Arctic Ocean, Mar. Chem. 231, 2021.

Yamamoto-Kawai, M., Carmack, E., Mclaughlin, F.: Nitrogen balance and Arctic throughflow, Nature 443, 43, 2006.

Yamamoto-Kawai, M., McLaughlin, F.A., Carmack, E.C., Nishino, S., Shimada, K.: Freshwater budget of the Canada Basin, Arctic Ocean, from salinity, d18O, and nutrients, J. Geophys. Res. 113, C01007, 2008.

Yamashita, Y. and Tanoue, E.: Production of bio-refractory fluorescent dissolved organic matter in the ocean interior, Nat. Geosci. 1, 579–582, 2008.

Yamashita, Y., Yagi, Y., Ueno, H., Ooki, A., and Hirawake, T.: Characterization of the water masses in the shelf region of the Bering and Chukchi Seas with fluorescent organic matter, J. Geophys. Res. Oceans 124, 7545–7556, 2019.

Table 1 Results of measurement of certified reference materials for the trace metals, NASS-7 and CASS-6.

Element	NASS-7 (μg kg^{-1})			CASS-6 (μg kg^{-1})		
	Analytical value		Certified value	Analytical value		Certified value
	n	average ± sd	average ± sd	*n*	average ± sd	average ± sd
Fe	4	0.366 ± 0.018	0.344 ± 0.026	4	1.47 ± 0.01	1.53 ± 0.12
Mn	4	0.75 ± 0.004	0.74 ± 0.06	4	2.15 ± 0.02	2.18 ± 0.12

765

Table 2 Endmember values of meteoric water, sea-ice meltwater, Pacific Water, and Atlantic Water for salinity, $\delta^{18}O$, and phosphate concentration based on the nitrate to phosphate ratio. *N* represents the measured value of nitrate+nitrite. The endmember value of sea-ice meltwater was obtained from this study, and others were obtained from the studies performed by
770 Bauch et al. (2011), Gerringa et al. (2021), Jones et al. (2008), and Newton et al. (2013).

Endmember	Salinity	$\delta^{18}O$ (‰)	phosphate (μmol kg^{-1})
Meteoric water (f_{mw})	0	–20	0.1
Sea-ice meltwater (f_{sim})	2.1	–2.08	0.06
Pacific Water ($f_{Pacific}$)	32.7	–1.1	$0.0653 \times N + 0.94$
Atlantic Water ($f_{Atlantic}$)	34.92	+0.3	$0.0596 \times N + 0.1139$

Table 3 Comparison of inventories of Fe and Mn (μmol m^{-2}) in sea ice core from the Arctic.

Samples	dFe	dMn	TdFe	TdMn	pFe	pMn	Reference
East Siberian Arctic Sea	1.6	3.3	4.8	3.7	–	–	This study
Canada Basin	2.7	5.5	137	4.8	–	–	Evans and Nishioka, 2019
Western-Central Arctic	–	–	–	–	11 to 63	0.4 to 1.5	Bolt et al., 2020

TdFe and TdMn were determined in acidified unfiltered samples.

pFe and pMn were determined in acid-digested particle samples.